

Variational Inference of Structured Line Spectra Exploiting Group-Sparsity

Jakob Möderl, Franz Pernkopf, Klaus Witrisal, Erik Leitinger

Abstract—In this paper, we present a variational inference algorithm that decomposes a signal into multiple groups of related spectral lines. The spectral lines in each group are associated with a group parameter common to all spectral lines within the group. The proposed algorithm jointly estimates the group parameters, the number of spectral lines within a group, and the number of groups exploiting a Bernoulli-Gamma-Gaussian hierarchical prior model which promotes sparse solutions. Aiming to maximize the evidence lower bound (ELBO), variational inference provides analytic approximations of the posterior probability density functions (PDFs) and also gives estimates of the additional model parameters such as the measurement noise variance. While the activation variables of the groups and the associated group parameters (such as fundamental frequencies and the corresponding higher order harmonics) are estimated as point estimates, the remaining parameters such as the complex amplitudes of the spectral lines and their precision parameters are estimated as approximate posterior PDFs.

We demonstrate the versatility and performance of the proposed algorithm on three different inference problems. In particular, the proposed algorithm is applied to the multi-pitch estimation problem, the radar signal-based extended object estimation problem, and variational mode decomposition (VMD) using synthetic measurements and to real multi-pitch estimation problem using the Bach-10 dataset. The results show that the proposed algorithm outperforms state-of-the-art model-based and pre-trained algorithms on all three inference problems.

Index Terms—line spectral estimation, sparse Bayesian learning, multi-pitch estimation, extended object detection, variational mode decomposition

I. INTRODUCTION

The problem of line spectral estimation (LSE) [1], i.e. estimating the frequencies and amplitudes of a superposition of complex exponential functions from noisy measurements, is ubiquitous in signal processing. Solutions to this problem are applicable in many areas of physics and engineering, including range and direction estimation in radar and sonar, speech and music analysis, wireless channel estimation, molecular dynamics and geophysical exploration. Furthermore, in many applications the spectral lines can be organized into groups which share underlying parameters. One such example is pitch estimation in speech or music analysis [2]–[5]. The signal of each speaker during voiced speech or each tone of an instrument exhibits a harmonic structure with spectral lines

This research was partly funded by the Austrian Research Promotion Agency (FFG) within the project SEAMAL Front (project number: 880598). Furthermore, the financial support by the Christian Doppler Research Association, the Austrian Federal Ministry for Digital and Economic Affairs and the National Foundation for Research, Technology and Development is gratefully acknowledged.

The authors are with the Signal Processing and Speech Communications Laboratory at Graz University of Technology, Graz, Austria. Klaus Witrisal and Erik Leitinger are further associated with the Christian Doppler Laboratory for Location-aware Electronic Systems.

at integer multiples of some base frequency. Another example in radar signal processing are extended objects, which give rise to multiple related target signals [6]. Transformed into the frequency domain, this results in multiple correlated lines [7]. Many other problems such as variational mode decomposition (VMD) [8] can be approximated by a structured line spectrum. In these examples, the number of groups as well as which spectral line belongs to which group (i.e. the group structure) is not known a priori and has to be estimated as well, further complicating the estimation process.

A. State of the Art

Common solutions to the LSE problem assume the number of spectral lines (i.e. the model order) is known and no relation exists between the spectral lines. Such examples include subspace based methods such as MUSIC [9] or ESPRIT [10] as well as the maximum likelihood (ML) method [11], [12]. If the model order is not known, a criterion such as the Bayesian information criterion (BIC) or the Akaike information criterion (AIC) can be used to select a model order from a set of candidate model orders [13]. However, this approach can be computationally expensive since a solution must be obtained for each considered model order before a particular solution is chosen.

Sparse signal reconstruction methods aim to reconstruct a signal based on a large dictionary matrix which is weighted with a sparse amplitude vector. Thus, the model order is estimated as part of the process, alleviating the issue. A prominent instance of dictionary based sparse signal reconstruction method is the least absolute shrinkage and selection operator (LASSO) [14], which is also called basis pursuit denoising [15]. Further methods include matching pursuit [16], sparse Bayesian learning (SBL) [17]–[19] and SPICE [20]. See [21], [22] for a detailed discussion about the similarities and differences of some of these methods. Many of these algorithms have been extended to include a group structure, such as the group-LASSO [23]–[26], blockwise sparse regression [27], block matching pursuit [28], group-SBL [29], [30], pattern-coupled SBL [31] and group-SPICE [32]. A disadvantage of using a fixed dictionary matrix is the spectral leakage induced by the model mismatch, which decreases the estimation performance [33], [34]. Thus, parametrized approaches have been developed such as the gridless-SPICE algorithm [35] and extensions of SBL to a continuous (i.e., infinite) dictionary matrix with super-resolution capability¹ [36]–[38].

¹We define super-resolution as the ability of an algorithm to resolve spectral lines even if their separation in the dispersion domain is below the intrinsic resolution of the measurement equipment exploiting continuous dictionary matrices.

A further development of SBL-based super-resolution methods specific to LSE is the VALSE algorithm [39], which estimates posterior distributions of the frequencies instead of point estimates. Note, that all sparse signal reconstruction methods with complex amplitudes can be reframed as a grouping approach, where each group consists of the real and imaginary part of each weight [40].

Methods to solve the LSE problem using a grouped approach can be found for the application of multi-pitch estimation. A few examples include a harmonic extension for the capon beamformer and the MUSIC principle, as well as an expectation-maximization (EM)-based estimator, see [4] for a collection of these methods. A more recent approach is based on block sparsity given a grid of fundamental frequencies [41]. However, since this approach is based on a fixed frequency grid, it suffers the same drawbacks as other sparse signal reconstruction methods with fixed dictionary matrices. To alleviate this issue, [42] proposes a block-sparse method for harmonic LSE based on a grouped continuous (infinite) dictionary matrix. Finally, [43] uses a Bayesian hierarchical model and proposes an adaptive factorization of the posterior. Contrary to this work, [43] is not explicitly based on sparsity.

B. Contribution

In this paper, we propose a variational inference algorithm that promotes group-sparsity by exploiting a hierarchical Bernoulli-Gamma-Gaussian model for structured line spectra. The proposed algorithm decomposes the signal into several groups of related spectral lines which share a common group parameter. Each common group parameter is expressed by a continuous (infinite) dictionary and each spectral line within each group is related to this common group parameter by a discrete (finite) dictionary. An example for such a structured line spectrum can be a mixture of harmonic signals, where each common group parameter represents the fundamental frequency and the lines within the group form a harmonic series of spectral lines at multiples of the fundamental frequency. The contributions of this work are as follows.

- We apply a layered hierarchical Bernoulli-Gamma-Gaussian model, combining the Bernoulli-Gaussian model of [39] with the Gamma-Gaussian model as it is usually used in SBL [18] to obtain a solution which is sparse on two levels: the number of groups and the number of spectral lines within each group. The number of groups as well as the size of each group are estimated jointly with the continuous and discrete dictionary parameters.
- We present a formulation that allows to consider different structural relations between the spectral lines in the model. Thus, the model can be applied to a variety of inference problems.
- We derive the relation between the threshold governing the sparsity of groups and the threshold governing the sparsity of spectral lines within a group. This simplifies the process of tuning these thresholds to the application at hand.
- We demonstrate performance advantages on three different inference problems—multi-pitch estimation, detecting

and estimating extended objects using radar signals and VMD—using simulated data.

- We investigate the performance of the proposed algorithm on real multi-pitch data by applying it to the publicly available Bach-10 dataset.

II. SIGNAL MODEL AND BAYESIAN FORMULATION

A. Signal Model

We consider an N -length signal vector $\mathbf{x} = [x(-\frac{N}{2}T_s) \ x((-\frac{N}{2}+1)T_s) \ \dots \ x((\frac{N}{2}-1)T_s)]^T \in \mathbb{C}^N$, which contains the values of some continuous function $x(t)$ sampled at instances $\mathbf{t} = [-\frac{N}{2}T_s \ (-\frac{N}{2}+1)T_s \ \dots \ (\frac{N}{2}-1)T_s]^T$ with regular sampling interval T_s . We assume that \mathbf{x} is a linear combination of spectral lines in noise, and the spectral lines can be structured into K groups as²

$$\mathbf{x} = \sum_{k=1}^K \sum_{l \in \mathcal{S}_k} \alpha_{k,l} \psi(\theta_k, l) + \boldsymbol{\epsilon}. \quad (1)$$

Each group consists of one or multiple spectral lines $\psi(\theta_k, l) = e^{j2\pi f_{k,l} t}$, also referred to as components, with frequencies $f_{k,l}$ related to the parameter θ_k by a finite discrete alphabet $l \in \mathcal{S}_k$.³ Furthermore, each spectral line $\psi(\theta_k, l)$ is weighted with an amplitude $\alpha_{k,l} \in \mathbb{C}$ and the signal is corrupted by additive white Gaussian noise (AWGN) $\boldsymbol{\epsilon}$. We assume $\boldsymbol{\epsilon}$ to be sampled from a Gaussian random process with double sided power-spectral density $N_0/2$. Hence, $\boldsymbol{\epsilon}$ follows a circular-symmetric complex Gaussian distribution, i.e., $p(\boldsymbol{\epsilon}) = \mathcal{CN}(\boldsymbol{\epsilon} | 0, \lambda^{-1} \mathbf{I})$ with precision $\lambda = \frac{1}{N_0}$.⁴

We aim to estimate the number of groups K , the fundamental frequencies θ_k , the group structure \mathcal{S}_k of each group, the amplitudes $\alpha_{k,l}$ and noise variance λ . Note, that the signal model in (1) can be straightforwardly extended to multiple measurement vectors such as signals from an microphone or antenna array and to vector parameters such as estimating the angle-of-arrival in addition to the fundamental frequency. Furthermore, any set of functions can be selected as basis instead of the structured spectral lines. Thus, the signal model is potentially applicable to an even wider variety of engineering problems.

B. Inference Model and Bayesian Formulation

To perform (approximate) Bayesian inference on this model, we rewrite (1) as product of a large parametrized dictionary matrix $\boldsymbol{\Psi}(\boldsymbol{\theta})$ whose columns contain all possible components of a large number of groups multiplied with a sparse

²As an illustrative example for a structured line spectrum consider a note with pitch f_0 played on an instrument. The line spectrum of the audio signal produced by the instrument is a harmonic series with spectral lines at multiples of f_0 , e.g. at $\{f_0, 2f_0, 3f_0, 4f_0, 5f_0\}$. We can model such a line spectrum using (1) by $K = 1$, $f_{k,l} = \theta_k l$, $\theta_1 = f_0$ and $\mathcal{S}_1 = \{1, 2, 3, 4, 5\}$. If several notes are played together to form a chord, the different harmonic series are superimposed on each other. Thus, the line spectrum will consist of $K > 1$ such harmonic series with different fundamental pitches each.

³ $e^{\mathbf{a}}$ with $\mathbf{a} = [a_1 \ a_2 \ \dots \ a_N]^T \in \mathbb{C}^N$ is defined to be a vector, i.e., $e^{\mathbf{a}} \triangleq [e^{a_1} \ e^{a_2} \ \dots \ e^{a_N}]^T$.

⁴We denote the complex Gaussian PDF of the variable $\mathbf{x} \in \mathbb{C}^N$ with mean $\boldsymbol{\mu}$ and covariance $\boldsymbol{\Sigma}$ as $\mathcal{CN}(\mathbf{x} | \boldsymbol{\mu}, \boldsymbol{\Sigma}) = |\pi \boldsymbol{\Sigma}|^{-1} \exp\{-(\mathbf{x} - \boldsymbol{\mu})^H \boldsymbol{\Sigma}^{-1} (\mathbf{x} - \boldsymbol{\mu})\}$, where $|\cdot|$ denotes the matrix determinant. Furthermore, we assume that $\mathbf{x} - \boldsymbol{\mu}$ is proper for all complex Gaussian random variables \mathbf{x} with mean $\boldsymbol{\mu}$.

amplitude vector α . Let $\mathcal{S}_{\max} = \{l \mid L_{\min} \leq l \leq L_{\max}\}$ be the set of all potential components of a group defined by L_{\min} and L_{\max} , and K_{\max} the maximum number of groups.⁵ Let $\theta = [\theta_1 \theta_2 \cdots \theta_{K_{\max}}]^T$ be a vector of the corresponding fundamental frequencies θ_k and $\Psi(\theta_k) = [\psi(\theta_k, L_{\min}) \psi(\theta_k, L_{\min} + 1) \cdots \psi(\theta_k, L_{\max})]$ a matrix whose columns contain all spectral lines parametrized by θ_k , and $\Psi(\theta) = [\Psi(\theta_1) \Psi(\theta_2) \cdots \Psi(\theta_{K_{\max}})]$. Furthermore, we introduce amplitude vectors for each possible group $\alpha_k = [\alpha_{k,L_{\min}} \alpha_{k,L_{\min}+1} \cdots \alpha_{k,L_{\max}}]^T$ and the sparse vector of all amplitudes $\alpha = [\alpha_1^T \alpha_2^T \cdots \alpha_{K_{\max}}^T]^T$. With this the inference model of the signal model in (1) is given by

$$\mathbf{x} = \Psi(\theta)\alpha + \epsilon. \quad (2)$$

To achieve sparsity on both levels, in the number of groups as well as in the number of components in each group, we propose to use a Bernoulli-Gamma-Gaussian prior model. We model the existence of each group with independent Bernoulli distributed random variables while simultaneously modeling the prior variance of each amplitude with Gamma distributed random variables. A factor graph representation of the model is depicted in Figure 1. Our model differs from [37], [38] in the addition of the Bernoulli-prior which is shown to increase resilience against the insertion of artificial components [39], while it differs from [36], [39] by using the Bernoulli-prior to model the existence of groups of several components instead of individual components. Note, that we can constrain each group to contain at most a single spectral line with frequency θ_k by setting $\mathcal{S}_{\max} = \{0\}$ and $f_{k,l} = \theta_k$. In this case, the hierarchical model is identical to [36]. Therefore, the presented method can be viewed as a generalization of [36], except we use a variational-EM inference scheme instead of maximizing a Type-II likelihood function [22]. We would like to emphasise here that the hierarchical model is just a ‘‘convenient fiction’’ in order to construct useful cost functions for penalized regression of the form

$$\hat{\theta}, \hat{\alpha} = \arg \min_{\theta, \alpha} \|\mathbf{x} - \Psi(\theta)\alpha\|^2 + g(\theta, \alpha) \quad (3)$$

where $g(\theta, \alpha)$ is a penalty term which promotes sparsity [22].

For each potential group $k \in \{1, 2, \cdots, K_{\max}\}$, we introduce binary random variables $\mathbf{z} = [z_1 z_2 \cdots z_{K_{\max}}]^T$, $z_k \in \{0, 1\}$ which select whether the k -th group is active or not. If the k -th group is not active all amplitudes are zero $\alpha_{k,l} = 0 \forall l$. The prior PDF of the amplitudes $\alpha_{k,l}$ of all active groups is further modeled by independent complex Gaussian PDFs with precisions $\gamma_{k,l}$, that are again treated as random variables and inferred as nuisance parameters [17], [18], [36]–[38]. Thus, the prior PDF for an individual amplitude $\alpha_{k,l}$ conditioned on z_k and $\gamma_{k,l}$ is then given by

$$p(\alpha_{k,l} | \gamma_{k,l}, z_k) = z_k \mathcal{CN}(\alpha_{k,l} | 0, \gamma_{k,l}^{-1}) + (1 - z_k) \delta(\alpha_{k,l}) \quad (4)$$

where $\delta(\cdot)$ is the Dirac delta function. The variables z_k represent sparsity-inducing priors on the group level and their

⁵Since we apply a bottom-up initialization and we can never expect to estimate more parameters than the number of observations, the actual values of L_{\min} , L_{\max} and K_{\max} do not influence the proposed algorithm as long as they allow for a large enough number of groups and components per group.

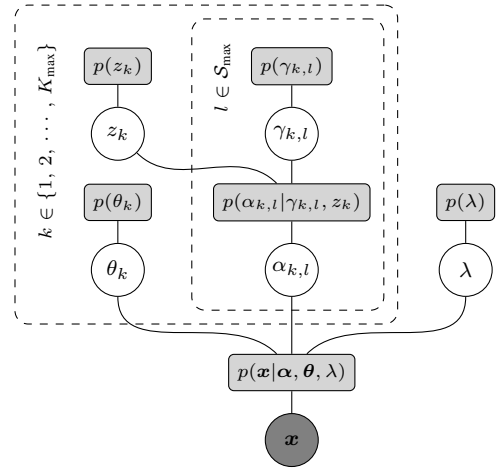


Fig. 1. Factor graph representation of the Bernoulli-Gamma-Gaussian model for sparse group estimates. Sparsity of components is promoted by Gamma PDFs as hyperpriors for $\gamma_{k,l}$, while sparsity in groups is promoted by Bernoulli PDFs as hyperpriors for z_k .

hyperpriors are modeled as independent Bernoulli PDFs with \bar{z} as probability for $z_k = 1$, i.e.,

$$p(\mathbf{z}) = \prod_{k=1}^{K_{\max}} \bar{z}^{z_k} (1 - \bar{z})^{1-z_k}. \quad (5)$$

The precisions $\gamma_{k,l}$ represent the prior variances for components within a group and their hyperpriors are modeled by independent Gamma PDFs $p(\gamma_{k,l}) = \text{Ga}(\gamma_{k,l} | \eta, \nu)$ with shape η and rate ν .⁶ Note that since the PDFs of the amplitude’s precisions $p(\gamma_{k,l})$ are sparsity inducing, the according hierarchical model leads to many component amplitudes having a prior variance of zero, resulting in them being removed from the model as the corresponding amplitude is estimated to be zero as well. The number of groups and number of components within a group are indirectly estimated by, respectively, estimating the posterior PDFs of z_k and $\gamma_{k,l}$.

Let $\gamma_k = [\gamma_{k,L_{\min}} \gamma_{k,L_{\min}+1} \cdots \gamma_{k,L_{\max}}]^T$ be a column-vector of the precisions $\gamma_{k,l}$ corresponding to the amplitudes α_k of the k -th group and $\gamma = [\gamma_1^T \gamma_2^T \cdots \gamma_{K_{\max}}^T]^T$ be a vector of all precisions $\gamma_{k,l}$. Let $\mathcal{S} = \mathcal{S}(\gamma, \mathbf{z})$ be an index set such that $\alpha_{\mathcal{S}}$ contains all nonzero elements of α and $\gamma_{\mathcal{S}}$ contains the prior variances corresponding the amplitudes $\alpha_{\mathcal{S}}$.⁷ Finally, let $\Gamma = \text{diag}(\gamma_{\mathcal{S}})$, where $\text{diag}(\gamma_{\mathcal{S}})$ denotes a diagonal matrix with the elements of the vector $\gamma_{\mathcal{S}}$ along the main diagonal, such that the joint prior PDF of the amplitudes is given by

$$p(\alpha | \gamma, \mathbf{z}) = \mathcal{CN}(\alpha_{\mathcal{S}} | \mathbf{0}, \Gamma^{-1}) \prod_{\alpha_{k,l} \notin \alpha_{\mathcal{S}}} \delta(\alpha_{k,l}). \quad (6)$$

We assume the prior distribution of the noise variance to be a Gamma PDF $p(\lambda) = \text{Ga}(\lambda | \rho, \mu)$ with shape ρ and rate μ , since this is the conjugate prior for the variance of a

⁶We denote the Gamma PDF with shape a and rate b as $\text{Ga}(x | a, b) = \frac{b^a}{\Gamma(a)} x^{a-1} e^{-bx}$, where $\Gamma(\cdot)$ is the gamma function.

⁷We denote a vector subscripted by an index set $\alpha_{\mathcal{S}}$ as the vector containing the elements of α whose indices are elements of \mathcal{S} . Similarly, we denote for matrices $\Psi_{\mathcal{S}}(\theta)$ as the matrix formed by the columns of $\Psi(\theta)$ whose indices are elements of \mathcal{S} .

Gaussian PDF. From the AWGN assumption it follows that the likelihood $p(\mathbf{x}|\boldsymbol{\alpha}, \boldsymbol{\theta}, \lambda)$ follows a Gaussian PDF

$$p(\mathbf{x}|\boldsymbol{\alpha}, \boldsymbol{\theta}, \lambda) = \mathcal{CN}(\mathbf{x} | \boldsymbol{\Psi}_{\mathcal{S}}(\boldsymbol{\theta})\boldsymbol{\alpha}_{\mathcal{S}}, \lambda^{-1}\mathbf{I}). \quad (7)$$

Introducing $p(\boldsymbol{\theta})$ as the prior for the parameters $\boldsymbol{\theta}$ and using the Bayes theorem, the posterior PDF is proportional to

$$p(\boldsymbol{\alpha}, \boldsymbol{\theta}, \boldsymbol{\gamma}, \boldsymbol{z}, \lambda | \mathbf{x}) \propto p(\mathbf{x}|\boldsymbol{\alpha}, \boldsymbol{\theta}, \lambda) p(\boldsymbol{\alpha}|\boldsymbol{\gamma}, \boldsymbol{z}) p(\boldsymbol{\gamma}) p(\boldsymbol{z}) p(\boldsymbol{\theta}) p(\lambda). \quad (8)$$

Calculating a maximum a-posteriori estimate from (8) is computationally prohibitive for all but the most simplest problems of interest due to the high dimensionality, interdependencies between variables and nonlinearities in the model. Thus, we apply a variational-EM approach [44], [45, Ch. 10] together with a structured mean-field assumption to approximate the posterior PDF.

III. VARIATIONAL APPROXIMATION

A. Mean-Field Factorization and Distribution Updates

We consider $\boldsymbol{\theta}$ and \boldsymbol{z} as deterministic unknowns and estimate point estimates $\hat{\boldsymbol{\theta}}$ and $\hat{\boldsymbol{z}}$, while we approximate the posterior distribution with a factorized proxy PDF given by

$$q(\boldsymbol{\alpha}, \boldsymbol{\gamma}, \lambda; \boldsymbol{\theta}, \boldsymbol{z}) = q_{\boldsymbol{\alpha}}(\boldsymbol{\alpha}; \boldsymbol{\theta}, \boldsymbol{z}) q_{\lambda}(\lambda; \boldsymbol{\theta}, \boldsymbol{z}) \times \prod_{k=1}^{K_{\max}} \prod_{l=L_{\min}}^{L_{\max}} q_{\boldsymbol{\gamma},k,l}(\boldsymbol{\gamma}_{k,l}; \boldsymbol{\theta}, \boldsymbol{z}) \quad (9)$$

parametrized by $\boldsymbol{\theta}$ and \boldsymbol{z} . This factorized PDF consists of a joint proxy PDF $q_{\boldsymbol{\alpha}}$ for all amplitudes and independent proxy PDFs $q_{\boldsymbol{\gamma},k,l}$ and q_{λ} for all prior variances $\gamma_{k,l}$ and the noise precision λ , respectively. We do not constrain the factors of the proxy PDF to be from a specific family. Thus, their shape is determined by the variational optimization procedure. We minimize the Kullback-Leibler (KL)-divergence between the true posterior PDF $p(\boldsymbol{\alpha}, \boldsymbol{\theta}, \boldsymbol{\gamma}, \boldsymbol{z}, \lambda | \mathbf{x})$ and the proxy PDF $q(\boldsymbol{\alpha}, \boldsymbol{\gamma}, \lambda; \boldsymbol{\theta}, \boldsymbol{z})$ by maximizing the evidence lower bound (ELBO) [44], [45, Ch. 10]

$$\mathcal{L}(q, \boldsymbol{\theta}, \boldsymbol{z}) = \langle \ln p(\boldsymbol{\alpha}, \boldsymbol{\theta}, \boldsymbol{\gamma}, \boldsymbol{z}, \lambda | \mathbf{x}) - \ln q(\boldsymbol{\alpha}, \boldsymbol{\gamma}, \lambda; \boldsymbol{\theta}, \boldsymbol{z}) \rangle_q \quad (10)$$

where $\langle f(x) \rangle_{q(x)}$ denotes the expectations of the function $f(x)$ with respect to the random variable x distributed according to the proxy PDF $q(x)$. We alternate between M-steps to maximize ELBO with respect to one or several of the proxy PDFs $q_j \in \mathcal{Q} = \{q_{\boldsymbol{\alpha}}, q_{\lambda}, q_{\boldsymbol{\gamma},1,L_{\min}}, q_{\boldsymbol{\gamma},1,L_{\min}+1}, \dots, q_{\boldsymbol{\gamma},K_{\max},L_{\max}}\}$, and E-Steps to maximize the ELBO with respect to the parameters $\hat{\boldsymbol{\theta}}$ and $\hat{\boldsymbol{z}}$, based on the updated proxy PDFs from the M-step. To avoid cluttered notation, we omit explicit iteration indices and refer to the last available estimates of the respective proxy PDFs and parameters.

In the M-step, each proxy PDF $q_j \in \mathcal{Q}$ is calculated according to

$$q_j \propto \exp \langle \ln p(\boldsymbol{\alpha}, \boldsymbol{\theta} = \hat{\boldsymbol{\theta}}, \boldsymbol{\gamma}, \boldsymbol{z} = \hat{\boldsymbol{z}}, \lambda | \mathbf{x}) \rangle_{\bar{q}_j} \quad (11)$$

where $\bar{q}_j = \prod_{q_i \in \mathcal{Q} \setminus q_j} q_i$ denotes the product of all factors of the joint proxy PDF q except q_j . Let $\hat{\boldsymbol{\gamma}}$ be the estimated mean

value of $\boldsymbol{\gamma}$ based on all $q_{\boldsymbol{\gamma},k,l}$ and $\hat{\mathcal{S}} = \mathcal{S}(\hat{\boldsymbol{\gamma}}, \hat{\boldsymbol{z}})$ the current estimate of \mathcal{S} . As we derive in Appendix A, inserting (8) into (11) results in the proxy PDFs

$$q_{\boldsymbol{\alpha}}(\boldsymbol{\alpha}; \hat{\boldsymbol{\theta}}, \hat{\boldsymbol{z}}) = \mathcal{CN}(\boldsymbol{\alpha}_{\mathcal{S}} | \hat{\boldsymbol{\alpha}}, \hat{\mathbf{C}}) \prod_{\alpha_{k,l} \notin \boldsymbol{\alpha}_{\mathcal{S}}} \delta(\alpha_{k,l}) \quad (12)$$

$$q_{\lambda}(\lambda; \hat{\boldsymbol{\theta}}, \hat{\boldsymbol{z}}) = \text{Ga}(\lambda | N + \rho, \hat{M}_{\lambda}) \quad (13)$$

$$q_{\boldsymbol{\gamma},k,l}(\boldsymbol{\gamma}_{k,l}; \hat{\boldsymbol{\theta}}, \hat{\boldsymbol{z}}) = \begin{cases} \text{Ga}(\boldsymbol{\gamma}_{k,l} | \eta + 1, \hat{M}_{k,l}) & \text{if } z_k = 1 \\ p(\boldsymbol{\gamma}_{k,l}) & \text{if } z_k = 0 \end{cases} \quad (14)$$

where \hat{M}_{λ} and $\hat{M}_{k,l}$ are the rate parameters of the resulting Gamma PDFs for q_{λ} and $q_{\boldsymbol{\gamma},k,l}$. If $\hat{z}_k = 0$, then $q_{\boldsymbol{\gamma},k,l}(\boldsymbol{\gamma}_{k,l}; \hat{\boldsymbol{\theta}}, \hat{\boldsymbol{z}}) = p(\boldsymbol{\gamma}_{k,l})$, which means that the whole group is deactivated based the Bernoulli-prior model. Let $\text{tr}(\cdot)$ denote the matrix trace operator, $\hat{\boldsymbol{\Psi}} = \boldsymbol{\Psi}_{\mathcal{S}}(\hat{\boldsymbol{\theta}})$ be the matrix of all spectral lines with nonzero amplitudes parametrized by $\hat{\boldsymbol{\theta}}$, $\hat{\boldsymbol{\Gamma}} = \text{diag}(\hat{\boldsymbol{\gamma}}_{\mathcal{S}})$ a diagonal matrix with the priors $\hat{\boldsymbol{\gamma}}_{k,l}$ of the active components on its main diagonal and $\hat{C}_{k,l}$ the element on the main diagonal of $\hat{\mathbf{C}}$ that corresponds to the estimated variance of the amplitude $\alpha_{k,l}$. Thus, the parameters of the proxy PDFs in (12), (13), and (14) are given, respectively, by

$$\hat{\boldsymbol{\alpha}} = \hat{\lambda} \hat{\mathbf{C}} \hat{\boldsymbol{\Psi}}^H \mathbf{x}, \quad (15)$$

$$\hat{\mathbf{C}} = (\hat{\lambda} \hat{\boldsymbol{\Psi}}^H \hat{\boldsymbol{\Psi}} + \hat{\boldsymbol{\Gamma}})^{-1}, \quad (16)$$

$$\hat{\lambda} = \frac{N + \rho}{\|\mathbf{x} - \hat{\boldsymbol{\Psi}} \hat{\boldsymbol{\alpha}}\|^2 + \text{tr}(\hat{\boldsymbol{\Psi}} \hat{\mathbf{C}} \hat{\boldsymbol{\Psi}}^H) + \mu}, \quad (17)$$

and

$$\hat{\boldsymbol{\gamma}}_{k,l} = \begin{cases} \frac{\eta+1}{\hat{C}_{k,l} + \|\hat{\boldsymbol{\alpha}}_{k,l}\|^2 + \nu} & \text{if } \hat{z}_k = 1 \\ \text{not defined} & \text{if } \hat{z}_k = 0 \end{cases}. \quad (18)$$

B. Fundamental Frequencies $\boldsymbol{\theta}$ and Group Activations \boldsymbol{z}

In order to estimate the fundamental frequencies $\hat{\boldsymbol{\theta}}$ and active groups $\hat{\boldsymbol{z}}$, the ELBO is maximized jointly with respect to $q_{\boldsymbol{\alpha}}$, $\boldsymbol{\theta}$, and \boldsymbol{z} [39]. In the following we use the product of all $q_{\boldsymbol{\gamma},k,l}$, i.e., $q_{\boldsymbol{\gamma}} = \prod_{k=1}^{K_{\max}} \prod_{l=L_{\min}}^{L_{\max}} q_{\boldsymbol{\gamma},k,l}$ and $\overset{\circ}{q}$, which means that the right side is equal to the left side plus a constant, such that both sides are proportional to each other after applying the exponential function. The ELBO in (10) for the proxy PDF $q_{\boldsymbol{\alpha}}$ is given by

$$\mathcal{L}(q_{\boldsymbol{\alpha}}, \boldsymbol{\theta}, \boldsymbol{z}) \overset{\circ}{=} \langle \langle \ln p(\boldsymbol{\alpha}, \boldsymbol{\theta}, \boldsymbol{\gamma}, \boldsymbol{z}, \lambda | \mathbf{x}) \rangle_{q_{\lambda} q_{\boldsymbol{\gamma}}} - \ln q_{\boldsymbol{\alpha}}(\boldsymbol{\alpha}; \boldsymbol{\theta}, \boldsymbol{z}) \rangle_{q_{\boldsymbol{\alpha}}}. \quad (19)$$

Since $\boldsymbol{\theta}$ and \boldsymbol{z} are restricted to point estimates, the standard free-form optimization [45, Ch. 10] is not applicable. Following [39], we introduce the PDF

$$t(\boldsymbol{\alpha}; \boldsymbol{\theta}, \boldsymbol{z}) = \frac{1}{Z(\boldsymbol{\theta}, \boldsymbol{z})} \exp \langle \ln p(\boldsymbol{\alpha}, \boldsymbol{\theta}, \boldsymbol{\gamma}, \boldsymbol{z}, \lambda | \mathbf{x}) \rangle_{q_{\lambda} q_{\boldsymbol{\gamma}}} \quad (20)$$

with normalization constant

$$Z(\boldsymbol{\theta}, \boldsymbol{z}) = \int_{\boldsymbol{\alpha}} \exp \langle \ln p(\boldsymbol{\alpha}, \boldsymbol{\theta}, \boldsymbol{\gamma}, \boldsymbol{z}, \lambda | \mathbf{x}) \rangle_{q_{\lambda} q_{\boldsymbol{\gamma}}} d\boldsymbol{\alpha}. \quad (21)$$

Using (20) and (21), the ELBO in (19) can be rewritten as

$$\mathcal{L}(q_{\boldsymbol{\alpha}}, \boldsymbol{\theta}, \boldsymbol{z}) = \text{const.} - \mathcal{D}_{\text{KL}}(q_{\boldsymbol{\alpha}} \| t) + \ln Z(\boldsymbol{\theta}, \boldsymbol{z}) \quad (22)$$

where $\mathcal{D}_{\text{KL}}(q||p)$ denotes the KL divergence of q from p . Since $\mathcal{D}_{\text{KL}} \geq 0$ with equality if and only if $t = q_\alpha$, (22) is maximized by

$$q_\alpha(\boldsymbol{\alpha}; \hat{\boldsymbol{\theta}}, \hat{\boldsymbol{z}}) = t(\boldsymbol{\alpha}; \hat{\boldsymbol{\theta}}, \hat{\boldsymbol{z}}) \quad (23)$$

where point estimates $\hat{\boldsymbol{\theta}}$ and $\hat{\boldsymbol{z}}$ are determined by

$$\hat{\boldsymbol{\theta}}, \hat{\boldsymbol{z}} = \arg \max_{\boldsymbol{\theta}, \boldsymbol{z}} \ln Z(\boldsymbol{\theta}, \boldsymbol{z}). \quad (24)$$

Let $\tilde{\mathcal{S}} = \mathcal{S}(\hat{\boldsymbol{\gamma}}, \boldsymbol{z})$, $\Psi_{\tilde{\mathcal{S}}} = \Psi_{\tilde{\mathcal{S}}}(\boldsymbol{\theta})$, $\hat{\Gamma}_{\tilde{\mathcal{S}}} = \text{diag}(\hat{\boldsymbol{\gamma}}_{\tilde{\mathcal{S}}})$ and $\mathbf{C}_{\tilde{\mathcal{S}}} = (\hat{\lambda} \Psi_{\tilde{\mathcal{S}}}^H \Psi_{\tilde{\mathcal{S}}} + \hat{\Gamma}_{\tilde{\mathcal{S}}})^{-1}$. As we derive in Appendix B, we find $\hat{\boldsymbol{\theta}}$ and $\hat{\boldsymbol{z}}$ from (24) as the maximizer of

$$\begin{aligned} \ln Z(\boldsymbol{\theta}, \boldsymbol{z}) &\stackrel{e}{\propto} \hat{\lambda}^2 \mathbf{x}^H \Psi_{\tilde{\mathcal{S}}} \mathbf{C}_{\tilde{\mathcal{S}}} \Psi_{\tilde{\mathcal{S}}}^H \mathbf{x} + \ln |\mathbf{C}_{\tilde{\mathcal{S}}}| + \ln p(\boldsymbol{z}) \\ &+ \sum_{\hat{\gamma}_{k,l} \in \tilde{\mathcal{S}}} \langle \ln \gamma_{k,l} \rangle_{q_{\gamma,k,l}} + \ln p(\boldsymbol{\theta}) \end{aligned} \quad (25)$$

which is similar to the Type-II cost function that is obtained by maximizing the marginalized likelihood [37]. Finding the global maximum over all possible values of $\boldsymbol{\theta}$ and \boldsymbol{z} is computationally prohibitive. Therefore, we express the dependence on one set of parameters z_k , θ_k explicitly and maximize (25) by coordinate ascent.

Let Ψ_k denote the columns of $\Psi_{\tilde{\mathcal{S}}}$ which correspond to the k -th group and let the index \bar{k} refer to all the columns of matrices, or elements of vectors, which do not correspond to the k -th group. Without loss of generality, we can reorder $\hat{\boldsymbol{\gamma}}_{\tilde{\mathcal{S}}} = [\hat{\boldsymbol{\gamma}}_{\bar{k}}^T \hat{\boldsymbol{\gamma}}_k^T]^T$, $\boldsymbol{\theta} = [\boldsymbol{\theta}_{\bar{k}}^T \boldsymbol{\theta}_k]^T$, $\boldsymbol{z} = [z_{\bar{k}}^T z_k]^T$, and $\Psi_{\tilde{\mathcal{S}}} = [\Psi_{\bar{k}} \Psi_k]$ such that the elements corresponding to the k -th group are moved to the end. Let $\hat{\Gamma}_{\bar{k}} = \text{diag}(\hat{\boldsymbol{\gamma}}_{\bar{k}})$, and $\hat{\Gamma}_k = \text{diag}(\hat{\boldsymbol{\gamma}}_k)$, $\mathbf{C}_{\bar{k}} = (\hat{\lambda} \Psi_{\bar{k}}^H \Psi_{\bar{k}} + \hat{\Gamma}_{\bar{k}})^{-1}$, $\mathbf{C}_k = (\hat{\lambda} \Psi_k^H \Psi_k + \hat{\Gamma}_k - \hat{\lambda}^2 \Psi_k^H \Psi_{\bar{k}} \mathbf{C}_{\bar{k}} \Psi_{\bar{k}}^H \Psi_k)^{-1}$, and $\mathbf{u} = \hat{\lambda} \mathbf{C}_k \Psi_k^H (\mathbf{I} - \hat{\lambda} \Psi_{\bar{k}} \mathbf{C}_{\bar{k}} \Psi_{\bar{k}}^H) \mathbf{x}$. As detailed in Appendix A, we assume the parameter priors $p(\boldsymbol{\theta})$ to be independent and flat, to express the difference between $\ln Z$ with the k -th group removed and $\ln Z$ including the k -th group as

$$\begin{aligned} \Delta_k(\theta_k) &= \ln Z([\hat{\boldsymbol{\theta}}_{\bar{k}}^T \boldsymbol{\theta}_k]^T, [z_{\bar{k}}^T \ 1]^T) - \ln Z([\hat{\boldsymbol{\theta}}_{\bar{k}}^T \boldsymbol{\theta}_k]^T, [z_{\bar{k}}^T \ 0]^T) \\ &= \mathbf{u}^H \mathbf{C}_k^{-1} \mathbf{u} + \ln |\mathbf{C}_k| + \ln \frac{\bar{z}}{1 - \bar{z}} + \sum_{l \in \hat{\mathcal{S}}_k} (\chi_0 + \ln \hat{\gamma}_{k,l}) \end{aligned} \quad (26)$$

where $\hat{\mathcal{S}}_k = \{l | \hat{\gamma}_{k,l} < \infty\}$ and $\chi_0 = \text{digamma}(\eta + 1)$ is the digamma function evaluated at $\eta + 1$. After finding $\hat{\theta}_k = \arg \max_{\theta_k} \Delta_k(\theta_k)$, we activate the k -th group by $\hat{z}_k = 1$ and update the respective parameter to $\hat{\theta}_k$ if $\Delta_k(\hat{\theta}_k) > 0$, indicating an increase in $\ln Z$ compared to deactivating the k -th group by $\hat{z}_k = 0$.

C. Fast Update of Priors $\gamma_{k,l}$ and Component Threshold χ_1

If the prior PDFs $p(\gamma_{k,l})$ is sparsity-inducing, many estimates $\hat{\gamma}_{k,l}$ will diverge if the updated equations (15) through (18) are iterated ad infinitum, resulting in a sparse estimate for $\hat{\boldsymbol{\alpha}}$ [17], [19]. To obtain a fast convergence check, we consider Jeffery's prior $p(\gamma_{k,l}) \propto \gamma_{k,l}^{-1}$ obtained by $\eta = \nu = 0$ and investigating the dependency of $\hat{\gamma}_{k,l}$ on $\hat{\boldsymbol{\alpha}}$ and $\hat{\mathbf{C}}$. Following [19], we can express repeated cycles of updating q_α followed by updating $q_{\gamma,k,l}$ as a nonlinear map. Inserting (15) and (16) into (18), each cycle i maps from the previous estimate

of $\hat{\gamma}_{k,l}$ to the next as $\hat{\gamma}_{k,l}^{[i]} = F(\hat{\gamma}_{k,l}^{[i-1]})$. Hence, we can derive fast update rules for $\gamma_{k,l}$ by analysing the stationary points of the map $F(\cdot)$. Let $\boldsymbol{\psi}_{k,l} = \boldsymbol{\psi}(\hat{\theta}_k, l)$, $\Psi_{\bar{k},l}$ be the dictionary matrix $\hat{\Psi}$ with the column $\boldsymbol{\psi}_{k,l}$ removed, $\hat{\Gamma}_{\bar{k},l}$ a diagonal matrix containing the elements of $\hat{\boldsymbol{\gamma}}_{\tilde{\mathcal{S}}}$ with $\hat{\gamma}_{k,l}$ removed and $\mathbf{C}_{\bar{k},l} = (\hat{\lambda} \Psi_{\bar{k},l}^H \Psi_{\bar{k},l} + \hat{\Gamma}_{\bar{k},l})^{-1}$. Furthermore, let $s_{k,l} = (\hat{\lambda} \boldsymbol{\psi}_{k,l}^H \boldsymbol{\psi}_{k,l} - \hat{\lambda}^2 \boldsymbol{\psi}_{k,l}^H \Psi_{\bar{k},l} \mathbf{C}_{\bar{k},l} \Psi_{\bar{k},l}^H \boldsymbol{\psi}_{k,l})^{-1}$ and $u_{k,l} = s_{k,l} (\hat{\lambda} \boldsymbol{\psi}_{k,l}^H \mathbf{x} - \hat{\lambda}^2 \boldsymbol{\psi}_{k,l}^H \Psi_{\bar{k},l} \mathbf{C}_{\bar{k},l} \Psi_{\bar{k},l}^H \mathbf{x})$, the map $F(\cdot)$ can be shown to converge to

$$\hat{\gamma}_{k,l} \triangleq \hat{\gamma}_{k,l}^{[\infty]} = (|u_{k,l}|^2 - s_{k,l})^{-1} \quad \text{if} \quad \frac{|u_{k,l}|^2}{s_{k,l}} > 1 \quad (27)$$

and diverges otherwise. Thus, if (27) is fulfilled we keep the l -th component of the k -th group in the model and discard it otherwise. A similar analysis can be performed for $\eta > 0$ and $\nu > 0$. However, for the sake of brevity we consider this analysis to be outside the scope of this work.

It can be shown that $\frac{|u_{k,l}|^2}{s_{k,l}}$ corresponds to the component signal-to-noise ratio (SNR) [19] and, thus, the condition $\frac{|u_{k,l}|^2}{s_{k,l}} > 1$ equals accepting any component that is even slightly above the noise level. However, this will also result in some false alarms. We can heuristically increase the threshold to $\frac{|u_{k,l}|^2}{s_{k,l}} > \chi_1 \geq 1$ in order to reduce the false alarm rate at the cost of an increased missed detection rate, where χ_1 corresponds to the minimum required component SNR. We refer the reader to [46] for a closer analysis of the relationship between the false alarm rate and the threshold in the case of unstructured line spectra. Note, that by increasing the threshold we lose the guarantee that each update step increases the ELBO and, thus, the guarantee for convergence. Nevertheless, increasing the threshold was not observed to impact the performance or convergence behaviour in a noticeable manner in our simulations.

D. Model Ambiguity and Constraints on Sparsity Parameters

The model (2) is ambiguous since many combinations of groups and active components within each group can lead to the same spectral lines. For example, if the components in each group are spectral lines with frequency $\theta_k l$, then each group can also be parametrized by $\theta'_k = \frac{\theta_k}{2}$ and $l' = 2l$. This effect is also known as the halfling problem [42]. We try to reduce this type of error by using a bottom-up initialization strategy as described in Section IV.

Furthermore, if several components are assigned to one group, we can always remove one component to form a new group, parametrized such that it results in the same spectral lines as before, increasing the degrees of freedom in the model. Intuitively, we need to be stricter in adding new groups to the model compared to adding components within a group to avoid over parametrization. Following [36], we express $\mathbf{C}_k = [(s_{k,l}^{-1} + \hat{\gamma}_{k,l})^{-1}] = \frac{s_{k,l}}{1 + \hat{\gamma}_{k,l} s_{k,l}}$ and $\mathbf{u} = \frac{u_{k,l}}{1 + \hat{\gamma}_{k,l} s_{k,l}}$ for a group containing only a single spectral line. From (26) it follows, that we activate such a group if

$$\frac{|u_{k,l}|^2}{s_{k,l}} \frac{1}{1 + \hat{\gamma}_{k,l} s_{k,l}} + \ln \frac{\hat{\gamma}_{k,l} s_{k,l}}{1 + \hat{\gamma}_{k,l} s_{k,l}} + \ln \frac{\bar{z}}{1 - \bar{z}} + \chi_0 > 0 \quad (28)$$

which depends not only on the component SNR $\frac{|u_{k,l}|^2}{s_{k,l}}$ but also on the prior $\hat{\gamma}_{k,l}$ and variance $s_{k,l}$. Comparing (28) to (27), we ensure that the inclusion of new groups with only a single component is penalized more than the inclusion of new components within a group by choosing the group existence prior \bar{z} such that

$$(1 + \hat{\gamma}_{k,l} s_{k,l}) \left(\ln \frac{1 + \hat{\gamma}_{k,l} s_{k,l}}{\hat{\gamma}_{k,l} s_{k,l}} + \ln \frac{1 - \bar{z}}{\bar{z}} - \chi_0 \right) > \chi_1 \quad (29)$$

holds for any value of $\hat{\gamma}_{k,l} s_{k,l}$. Since $\hat{\gamma}_{k,l}$ and $s_{k,l}$ are both strictly positive quantities we have $(1 + \hat{\gamma}_{k,l} s_{k,l}) > 1$ and $\ln \frac{1 + \hat{\gamma}_{k,l} s_{k,l}}{\hat{\gamma}_{k,l} s_{k,l}} > 0$. Thus, (29) holds for any value of

$$\bar{z} < \frac{1}{1 + \exp(\chi_0 + \chi_1)}. \quad (30)$$

Finally, we express the cluster existence prior in terms of a second threshold χ_2 as $\bar{z} = \frac{1}{1 + \exp(\chi_0 + \chi_2)}$, which has to satisfy $\chi_2 > \chi_1$, for easier interpretation.

IV. ALGORITHM IMPLEMENTATION

Updating the parameters $\hat{\theta}$ and \hat{z} as well as the proxy distributions $q_j \in \mathcal{Q}$ in the way described in the previous section will converge towards a local optimum of the ELBO. However, there might exist several local optima and the obtained solution depends on the initialization as well as the order in which the updates are performed. In this section, we define an iterative schedule for updating the factors q_α , q_λ and $q_{\gamma,k,l}$ and to estimate $\hat{\theta}$ and \hat{z} as well as an initialization. The resulting algorithm is outlined in Algorithm 1. We choose Jeffrey's priors ($\rho = \mu = \eta = \nu = 0$) for $p(\gamma_{k,l})$ and $p(\lambda)$, since these priors are non informative for the noise precision and it allows us to use the fast convergence check developed in Section III-C for the variances $\hat{\gamma}_{k,l}$.

Without loss of generality, we can reorder the groups such that $\hat{z} = [1 \cdots 1 0 \cdots 0]$ is a vector of \hat{K} leading ones followed by $K_{\max} - \hat{K}$ zeros. Therefore, we only need to keep track of the estimated number of active groups \hat{K} and their parameters $\hat{\theta}_1$ through $\hat{\theta}_{\hat{K}}$ instead of the full vectors \hat{z} and $\hat{\theta}$. Similarly, instead of keeping the full vectors $\hat{\gamma}_k$, we keep track only of the priors $\hat{\gamma}_{k,l} < \infty$ and denote their respective indices with index sets \hat{S}_k for all $k \in \{1, 2, \dots, \hat{K}\}$. We start with an empty model (bottom-up initialization) where $\hat{K} = 0$, $\hat{\theta}$, $\hat{\gamma}$ and $\hat{\alpha}$ are empty vectors, and \hat{C} is an empty matrix. The noise precision is initialized using the signal energy as $\hat{\lambda} = \frac{N}{\|\mathbf{x}\|^2}$. Then, we repeatedly alternate between searching a for new group of components to add to the model and updating the already existing groups. We stop the procedure when the change in $\hat{\mathbf{x}} = \hat{\Psi} \hat{\alpha}$ from one iteration to the next is below a threshold and the search does not find a new group to add to the model.

To search for a new group, we would ideally find a combination of $\hat{\theta}_{\hat{K}+1}$ and $\hat{\gamma}_{\hat{K}+1}$ which maximizes $\hat{\theta}_{\hat{K}+1} = \arg \max_{\theta} \Delta_{\hat{K}+1}(\theta)$. Since this is computationally prohibitive, we choose a single component $l \in \mathcal{S}_{\max}$, e.g. $l = 1$, and consider a new group parametrized by $\theta_{\hat{K}+1} = \arg \max_{\theta} |\psi^H(\theta, l) \hat{\mathbf{x}}_{\text{res}}|$, where $\hat{\mathbf{x}}_{\text{res}} = \mathbf{x} - \hat{\Psi} \hat{\alpha}$ is the residual signal. Next, we perform Algorithm 2 to find other related

Algorithm 1 Main

Input: Signal vector \mathbf{x} .

Output: Model order \hat{K} , parameters $\hat{\theta}$, and amplitudes $\hat{\alpha}$.

Initialize $\hat{K} = 0$, $\hat{\lambda} = \frac{N}{\|\mathbf{x}\|^2}$, and $\hat{\alpha}$, $\hat{\theta}$, $\hat{\gamma}$ as empty vectors.

repeat

$\hat{\mathbf{x}}_{\text{res}} \leftarrow \mathbf{x} - \hat{\Psi} \hat{\alpha}$.

$\hat{\theta}_{\hat{K}+1} \leftarrow \arg \max_{\theta} |\psi^H(\theta, 1) \hat{\mathbf{x}}_{\text{res}}|$.

Perform Alg. 2 to estimate priors $\hat{\gamma}_{\hat{K}+1}$ and $\hat{S}_{\hat{K}+1}$.

Calc $\Delta_{\hat{K}+1}(\hat{\theta}_{\hat{K}+1})$ from (26)

if $\Delta_{\hat{K}+1}(\hat{\theta}_{\hat{K}+1}) > 0$ **then**

$\hat{K} \leftarrow \hat{K} + 1$.

$\hat{\theta} \leftarrow [\hat{\theta}^T, \hat{\theta}_{\hat{K}+1}]^T$, $\hat{\gamma} \leftarrow [\hat{\gamma}^T, \hat{\gamma}_{\hat{K}+1}]^T$.

end if

for all groups $k \in \{1, 2, \dots, \hat{K}\}$ **do**

Perform Alg. 2 to update priors $\hat{\gamma}_k$ and \hat{S}_k .

Find $\hat{\theta}_k = \arg \max_{\theta_k} \Delta_k(\theta_k)$ from (26).

if $\Delta_k(\hat{\theta}_k) \leq 0$ **then**

$\hat{K} \leftarrow \hat{K} - 1$, $\hat{\theta} \leftarrow \hat{\theta}_{\hat{K}}$, $\hat{\gamma} \leftarrow \hat{\gamma}_{\hat{K}}$.

end if

end for

Compute $\hat{\alpha}$ and \hat{C} from (15) and (16).

Compute $\hat{\lambda}$ from (17).

until stopping criterion.

Algorithm 2 Fast update of priors $\hat{\gamma}_k$

Input: Signal vector \mathbf{x} , parameters $\hat{\theta}$, $\hat{\gamma}$, \hat{S}_k , $\hat{\lambda}$, index k .

Output: Prior precisions $\hat{\gamma}_k$ and \hat{S}_k of the k -th group.

for all Components $l \in \hat{S}_k$ **do**

$s_{k,l} \leftarrow (\hat{\lambda} \psi_{k,l}^H \psi_{k,l} - \hat{\lambda}^2 \psi_{k,l}^H \Psi_{k,l} \mathbf{C}_{k,l} \Psi_{k,l}^H \psi_{k,l})^{-1}$.

$u_{k,l} \leftarrow s_{k,l} (\hat{\lambda} \psi_{k,l}^H \mathbf{x} - \hat{\lambda}^2 \psi_{k,l}^H \Psi_{k,l} \mathbf{C}_{k,l} \Psi_{k,l}^H \mathbf{x})$.

if $\frac{|u_{k,l}|^2}{s_{k,l}} > \chi_1$ **then**

$\hat{\gamma}_{k,l} \leftarrow (|u_{k,l}|^2 - s_{k,l})^{-1}$.

else

Remove $\hat{\gamma}_{k,l}$ from $\hat{\gamma}_k$.

$\hat{S}_k \leftarrow \hat{S}_k \setminus \{l\}$.

end if

end for

for all Components $l \in \mathcal{S}_{\text{search}} \setminus \hat{S}_k$ **do**

$s_{k,l} \leftarrow (\hat{\lambda} \psi_{k,l}^H \psi_{k,l} - \hat{\lambda}^2 \psi_{k,l}^H \hat{\Psi} \hat{C} \hat{\Psi}^H \psi_{k,l})^{-1}$.

$u_{k,l} \leftarrow s_{k,l} (\hat{\lambda} \psi_{k,l}^H \mathbf{x} - \hat{\lambda}^2 \psi_{k,l}^H \hat{\Psi} \hat{C} \hat{\Psi}^H \mathbf{x})$.

if $\frac{|u_{k,l}|^2}{s_{k,l}} > \chi_1$ **then**

$\hat{\gamma}_k \leftarrow [\hat{\gamma}_k^T, (|u_{k,l}|^2 - s_{k,l})^{-1}]^T$.

$\hat{S}_k \leftarrow \hat{S}_k \cup \{l\}$.

end if

end for

components in the proposed group and calculate the priors $\hat{\gamma}_{\hat{K}+1}$ for this new group. Finally, we add the group to the model if $\Delta_{\hat{K}+1}(\hat{\theta}_{\hat{K}+1}) > 0$.

After adding a new group, we iterate over all groups $k \in \{1, 2, \dots, \hat{K}\}$ and for each one we first perform an E-step to update the distributions $q_{\gamma,k,l}$, followed by an M-step to update $\hat{\theta}_k$ and \hat{z}_k . Lastly, we update the amplitude and noise distributions q_α and q_λ . The update of the distributions $q_{\gamma,k,l}$ is

outlined in Algorithm 2 and entails both updating the prior of existing components $\hat{\gamma}_{k,l}$ for all $l \in \hat{\mathcal{S}}_k$ as well as looking for new components to add to the group. Intuitively, we would calculate $u_{k,l}$ and $s_{k,l}$ for all $l \in \mathcal{S}_{\max}$ to check whether the component should be added or kept in the group or if it should be discarded. However, depending on the application and our choice of \mathcal{S}_{\max} this could be suboptimal. Consider the case of extended object detection. Since we do not want to constrain the size of each object, we are encouraged to use a large range for \mathcal{S}_{\max} . However, if two small objects are close to each other this would potentially result in the estimation of only a single group covering both objects with a few spectral lines deactivated in the middle. To prevent this, we can constrain the search space to $\mathcal{S}_{\text{search}} \subseteq \mathcal{S}_{\max}$ depending on the application. A reasonable choice for the example of extended object detection is to look for new components only in the neighbourhood of the currently existing ones by setting $\mathcal{S}_{\text{search}} = \{\min(\hat{\mathcal{S}}_k)-1, \min(\hat{\mathcal{S}}_k), \dots, \max(\hat{\mathcal{S}}_k)+1\} \cap \mathcal{S}_{\max}$. If such a constrained search space is used, it can be beneficial to run a few updates of each group before adding a new group in order to explore the search space quicker and avoid introducing new groups for components which would be covered by another existing group anyway.

V. APPLICATIONS AND RESULTS

A. Multi-pitch estimation

Multi-pitch estimation is a fundamental problem in audio signal processing [2]–[5], [41], [42]. The goal of multi-pitch estimation is to decompose the signal into several sources, each of which is modeled as a sum of harmonics, giving rise to the harmonically structured model

$$\mathbf{x} = \sum_{k=1}^K \sum_{l \in \mathcal{S}_k} \alpha_{k,l} e^{j2\pi l f_{0,k} t} + \epsilon. \quad (31)$$

Note that (31) is an instance of (1) since the multiples of the fundamental frequencies can be rewritten as $f_{k,l} = \theta_k l$ with $\theta_k = f_{0,k}$. We aim to estimate the number of sources K along with the fundamental frequency $f_{0,k}$ of each source while $\alpha_{k,l}$ and \mathcal{S}_k are considered nuisance parameters. Even though audio signals are typically real-valued, we can apply the complex-valued signal model by computing the (down-sampled) discrete-time analytical signal [47].

To adapt the proposed algorithm to multi-pitch estimation, we refine the search strategy to fit the task at hand. When looking for new components, we consider all harmonics up to a relative frequency of $\theta_k l = 1$. Thus, we use $\mathcal{S}_{\text{search}} = \{1, 2, \dots, \text{floor}(\frac{1}{\theta_k})\}$. To find the true fundamental frequency, we also perform a fractional search during which we search for components at fractions $l' \in \{\frac{1}{2}, \frac{1}{3}, \dots, \frac{1}{\text{floor}(N\hat{\theta}_k)}\}$ of the current estimate. If we find one such component we stop the fractional search and add l' to $\hat{\mathcal{S}}_k$. In order to obtain integer relations between all components we then re-parametrize $\hat{\theta}'_k = \hat{\theta}_k l'$ and $\hat{\mathcal{S}}'_k = \frac{\hat{\mathcal{S}}_k}{l'}$.

1) *Numerical Analysis:* To highlight the robustness of our algorithm against AWGN, we generate a signal of length $N = 100$ samples. For $N_{\text{MC}} = 1000$ simulation runs, the fundamental frequencies of $K = 2$ sources with 6 harmonics

each are drawn uniformly from the interval $[0.025, 0.1]$. If the fundamental frequencies are closer than $\frac{2}{N} = 0.02$, they are discarded and a new set of fundamental frequencies is drawn. We use the optimal subpattern assignment (OSPA) metric [48] to evaluate the estimation accuracy and cardinality errors of the estimated fundamental frequencies in a single metric. The cutoff-distance for the metric was set to $c = \frac{2}{N} = 0.02$ and the order parameter was set to $p = 1$.

A uniform prior $p(\theta_k) = \mathcal{U}(\theta_k | \frac{1}{N}, 1)$ over the full frequency range was applied for the proposed algorithm and the thresholds for component and group sparsity are set to $\chi_1 = 7$ dB and $\chi_2 = 10$ dB, respectively.⁸ We compare our algorithm to the BSURE-IR⁹ algorithm [42] and the approximate nonlinear-least-squares (ANLS) EM¹⁰ algorithm of [5]. The BSURE-IR algorithm was initialized with a grid of 15 frequency points in the interval $[0.025, 0.1]$ and the maximum allowed harmonic order was set to 6. The search interval for the ANLS-EM algorithm was set to $[0.025, 0.1]$ and an FFT size of 2^{12} was used.

Figure ?? shows the mean OSPA for all three algorithms versus the SNR defined as $\text{SNR} = \frac{\|\mathbf{x} - \epsilon\|^2}{\|\epsilon\|^2}$. The BSURE-IR algorithm was not able to find any fundamental frequencies for SNRs < 10 dB, as indicated by the OSPA being equal to the cutoff-distance c . Even for high SNRs of 20 dB and more, the performance of BSURE-IR was worse than that of the proposed algorithm. The performance of the ANLS-EM algorithm is similar to the proposed algorithm. For low SNRs of 5 dB and less the ANLS-EM outperforms the proposed algorithm in this example. However, both comparison algorithms have larger average runtime (averaged over simulation runs) than the proposed algorithm. The average runtime of the BSURE-IR algorithm strongly depends on the SNR. It is varying from 2.0 seconds for SNR = 20 dB to 19.3 seconds for SNR = 5 dB. In contrast, the average runtimes of the proposed algorithm and the ANLS-EM algorithm are approximately constant over the SNR with 0.1 seconds for the proposed method and 5.0 seconds for the ANLS-EM algorithm.

As a second experiment, we generate $N_{\text{MC}} = 1000$ simulations runs of a signal consisting of three notes with pitch f_0 , $\frac{5}{4}f_0$ and $\frac{3}{2}f_0$, i.e. a major triad with perfect temperament and $N = 100$ samples. Each note consists of six harmonics drawn randomly from $\{1, 2, \dots, 7\}$. The fundamental frequency of the base note f_0 was drawn uniformly random from the interval $[0.07, 0.08]$ and all harmonics are generated with unit amplitude and uniformly random phase. The BSURE-IR algorithm was initialized with 15 grid points in the interval $[0.06, 0.13]$ while the ANLS-EM algorithm was given the same range as frequency prior and the FFT-size was again set to 2^{12} . The settings for the proposed algorithm are the same as in the previous experiment. Figure ?? shows again the mean OSPA versus the SNR. In this scenario the proposed algorithm performs better than ANLS-EM algorithm for almost all SNR values. This is mainly due to the fact

⁸We denote the uniform PDF as $\mathcal{U}(x|a, b) = \frac{1}{b-a}$ for $a \leq x \leq b$ and 0 otherwise.

⁹https://www.maths.lu.se/fileadmin/maths/personal_staff/Andreas_Jakobsson/BSURE.zip

¹⁰<https://www.morganclaypool.com/page/multi-pitch>

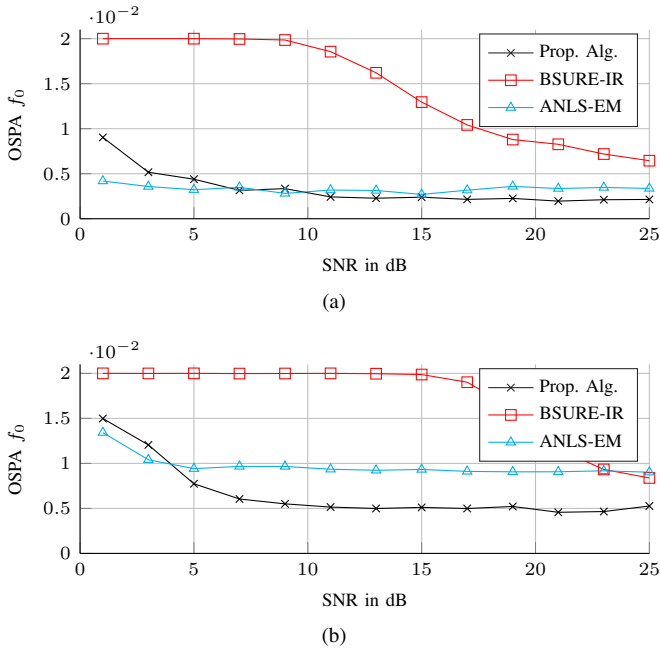


Fig. 2. OSPA of the estimated fundamental frequencies of a signal containing (a) 2 harmonic sources with fundamental frequencies drawn randomly from the interval $[0.025, 0.1]$ and (b) a major tritone with fundamental frequencies f_0 , $\frac{5}{4}f_0$ and $\frac{3}{2}f_0$.

that the ANLS-EM algorithm underestimates the model order in most cases, even for high SNR values of 20 dB and more. This indicates a performance degradation of the ANLS-EM algorithm in more complex scenarios containing more fundamental frequencies and overlapping harmonics. Again, The performance of BSURE-IR is the worst of the three, even in the high SNR regime.

2) *Real Music Signals*: To evaluate the performance of the proposed algorithm on real data, we apply it to estimate the fundamental pitches in the Bach-10 dataset¹¹ [49]. The dataset contains 10 chorales of J.S. Bach played by a quartet consisting of a violin, a clarinet, a saxophone and a bassoon. Each piece lasts between 25-40 seconds with all instruments playing nearly all the time. The audio of each instrument was recorded individually while the musician listened to the others via headphones. The fundamental pitch of each instrument was extracted from the individual recordings using the YIN single pitch estimator [50] as ground truth. Obvious errors in the ground truth are corrected manually. The audio signal was segmented into frames of 45 ms with a 10 ms stride between frames and the proposed algorithm was applied to each frame individually. Since the audio quality is quite good, we select the thresholds to be $\chi_1 = 15$ dB and $\chi_2 = 21$, dB, respectively, and applied a uniform prior between 75 Hz and 10 kHz. Each pitch in the ground truth was considered matched if an estimated pitch deviated from it no more than a halve of a semitone, i.e. if it deviates no more than 3% from the true pitch. Let $TP^{(i)}$ be the number of pitches matched between the ground truth and the estimate in each frame $i \in \{1, 2, \dots, N_{\text{Frames}}\}$, $FP^{(i)}$ the number of false positives, i.e. the number of estimated pitches which did not match to

¹¹<https://labsites.rochester.edu/air/resource.html>

TABLE I
PERFORMANCE MEASURES FOR THE PROPOSED ALGORITHM EVALUATED ON THE BACH-10 DATASET

Method	F ₁	Accuracy	Precision	Recall	Pre-Trained
Prop. Alg.	0.72	0.56	0.73	0.70	No
BW15	0.67	0.52	0.68	0.68	Yes
BSURE-IR	0.64	0.47	0.68	0.54	No
PEARLS	0.60	0.44	0.56	0.51	No

a ground truth pitch, and $FN^{(i)}$ the number of ground truth pitches which were not matched to an estimate, and N_{Frames} the total number of frames. Table I lists the accuracy, precision, recall and the F₁ of the proposed algorithm along with several comparison methods. The values were calculate using [51]

$$\text{Accuracy} = \frac{\sum_{i=1}^{N_{\text{Frames}}} TP^{(i)}}{\sum_{i=1}^{N_{\text{Frames}}} TP^{(i)} + FP^{(i)} + FN^{(i)}} \quad (32)$$

$$\text{Precision} = \frac{\sum_{i=1}^{N_{\text{Frames}}} TP^{(i)}}{\sum_{i=1}^{N_{\text{Frames}}} TP^{(i)} + FP^{(i)}} \quad (33)$$

$$\text{Recall} = \frac{\sum_{i=1}^{N_{\text{Frames}}} TP^{(i)}}{\sum_{i=1}^{N_{\text{Frames}}} TP^{(i)} + FN^{(i)}} \quad (34)$$

$$F_1 = \frac{2 \cdot \text{Precision} \cdot \text{Recall}}{\text{Precision} + \text{Recall}} \quad (35)$$

The comparison methods are two model based methods, BSURE-IR [42] and PEARLS [52], as well as a pretrained method [53] denote here as BW15. The results for BW15 are take from [52] since they reported an overall better accuracy for the method compared to the original paper. The ANLS-EM was not included in the table, since preliminary investigations showed a significantly worse performance on the dataset than the other algorithms, highlighting again the inability of the algorithm to cope with more complicated scenarios. Figure 3 shows the ground truth as well as the estimated fundamental frequencies obtained by the proposed algorithm for several frames of the choral “*Ach Gott und Herr*” of the dataset. The proposed algorithm is able to capture most of the fundamental frequencies with very few false positives and it outperforms all three state-of-the-art comparison methods, even BW15 that is pre-trained on the instruments in the dataset.

We considered only methods which work on the basis of individual frames to keep the comparison fair. Naturally, there exist several methods for multi-pitch estimation which not only estimate the pitches on a frame-by-frame basis but track notes over multiple frames to increase the performance. Thereby, these methods are able to achieve an F₁ score of up to 0.85 on the Bach 10 dataset. See e.g. [54] and references therein. However, these methods are usually data-driven and specifically tailored to multi-pitch estimation whereas our algorithm is the best purely model-based algorithm without being specifically tailored to the problem at hand. Furthermore, we also expect the proposed algorithm to generalize better to new datasets, out-of-domain data or noisy input data than data-driven approaches. Additionally, we expect that the performance of the proposed algorithm can be increased significantly by fusing information between frames.

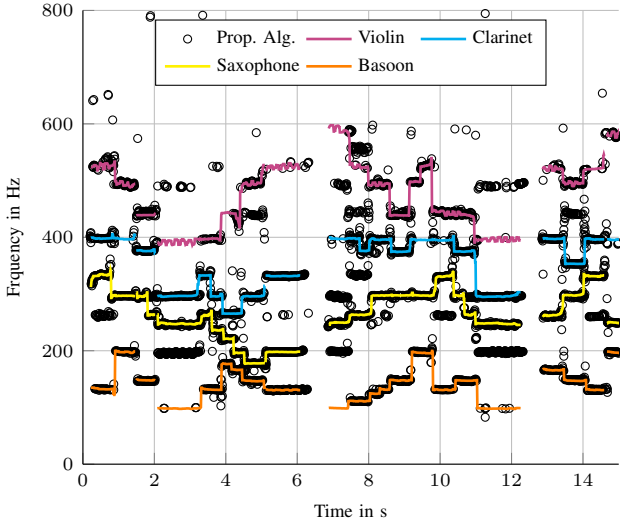


Fig. 3. Pitch estimates for 15 seconds of the choral *Ach Gott und Herr* compared to the ground truth (best viewed in color). The performance of the proposed algorithm for the depicted timespan is accuracy = 0.55, precision = 0.75 and recall = 0.68.

B. Extended Object Detection

A well-studied problem in radar signal processing is the detection of extended objects [6], [7]. An extended object is defined as a volume over which scatter points are distributed which correspond to a single physical target such as a car. The transmitted signal $s(t)$ is reflected by each of L_k scatter points of the k -th target and reaches the receiving antenna with some delay $\tau_{k,l} > 0$ with some amplitude $\alpha_{k,l} \in \mathbb{C}$. Thus, the received baseband signal can be modeled as

$$r(t) = \sum_{k=1}^K \sum_{l=1}^{L_k} \alpha_{k,l} s(t - \tau_{k,l}) + \epsilon(t). \quad (36)$$

Let $\Delta f = \frac{1}{N T_s}$, $R(f)$ be the Fourier transform of $r(t)$ and $\mathbf{r} = [R(-\frac{N}{2}\Delta f) R(-\frac{N}{2} + 1)\Delta f) \cdots R((\frac{N}{2} - 1)\Delta f)]^T$. Similarly, let $S(f)$ be the Fourier transform of $s(t)$, $\mathbf{s} = [S(-\frac{N}{2}\Delta f) S(-\frac{N}{2} + 1)\Delta f) \cdots S((\frac{N}{2} - 1)\Delta f)]^T$ and ϵ be a sampled vector of the noise in frequency domain. Furthermore, let $\mathbf{f} = [-\frac{N}{2}\Delta f (-\frac{N}{2} + 1)\Delta f \cdots (\frac{N}{2} - 1)\Delta f]^T$. We can then express (36) in the frequency domain as

$$\mathbf{r} = \sum_{k=1}^K \sum_{l=1}^{L_k} \alpha_{k,l} \mathbf{s} \odot e^{-j2\pi \mathbf{f} \tau_{k,l}} + \epsilon. \quad (37)$$

If the pulse is sufficiently short in time domain, we can apply the sampling theorem to approximate (36) with a few signal samples (“tabs”) spaced with delay $\Delta\tau = \frac{1}{f_s}$. Thus, (37) is well approximated by

$$\mathbf{r} = \sum_{k=1}^K \sum_{l=0}^{L'_k} (\mathbf{s} \odot e^{-j2\pi \mathbf{f} (\tau_{0,k} + l\Delta\tau)}) \alpha_{k,l} + \epsilon \quad (38)$$

where $\tau_{0,k} = \min_l(\tau_{k,l})$ is the smallest delay of the k -th target signal. Since the model (38) is an instance of (1), the proposed algorithm can be applied for the detection and estimation of the radar response from extended objects using $\theta_k = \tau_{0,k}$, $\psi(\tau_{0,k}, l) = \mathbf{s} \odot e^{-j2\pi \mathbf{f} \tau_{k,l}}$ and $\tau_{k,l} = \tau_{0,k} + l\Delta\tau$.

In order to showcase the ability of the algorithm to detect weak object signals and estimate their properties, we consider the case of a single object in noise and run a numerical experiment of $N_{MC} = 10^5$ realizations. The object is modeled according to [7] with a uniform intensity function $q(\tau)$ such that on average 10 scatter point are drawn between $\tau = 32.323 T_s$ to $\tau = 37.323 T_s$. Each scatter point was modeled to have an amplitude $\alpha_{k,l} \sim \mathcal{CN}(\alpha_{k,l}|0, 1)$ drawn independently from a complex Gaussian distribution with zero mean and unit variance.

To apply the proposed algorithm to the problem, we select $\mathcal{S}_{\text{search}} = \{\min(\hat{\mathcal{S}}_k) - 1, \min(\hat{\mathcal{S}}_k), \dots, \max(\hat{\mathcal{S}}_k) + 1\}$ and set the threshold to $\chi_1 = 3$ dB and $\chi_2 = 4$ dB. As comparison algorithms, we use two variants of SBL-based superresolution algorithms, the algorithm proposed in [38] abbreviated FV-SBL and the algorithm proposed in [36] abbreviated SF-SBL. Note that the SF-SBL is similar to the proposed algorithm using $\mathcal{S}_{\text{max}} = \{0\}$ (i.e. allowing only a single component per group) and $\chi_1 = 0$ dB. To make the comparison fair, we selected the thresholds of the three algorithms such the mean number of components estimated outside the object region, was approximately the same. Numerical analysis revealed that this is achieved by thresholds of 6 dB for the FV-SBL and $\chi_2 = 3.5$ dB for the SF-SBL. To estimate the extent \hat{O}_E and center-of-mass \hat{O}_C of the object we used an “oracle” data association which considered all components within ± 1 sample of the true object region to belong to the object and ignored the grouping estimated by the proposed algorithm. This data association is intended to reflect the information which can be obtained in case the algorithm is used to preprocess measurements for an extended object tracking filter which performs the data association. Let $\hat{\alpha}_{o,l}$ and $\hat{\tau}_{o,l}$ for $l \in \{1, 2, \dots, \hat{L}\}$ denote respective amplitudes and delays associated with the object, we estimated \hat{O}_E and \hat{O}_C as

$$\hat{O}_E = \max_l(\hat{\tau}_{o,l}) - \min_l(\hat{\tau}_{o,l}) \quad (39)$$

$$\hat{O}_C = \frac{\sum_{l=1}^{\hat{L}} |\hat{\alpha}_{o,l}|^2 \hat{\tau}_{o,l}}{\sum_{l=1}^{\hat{L}} |\hat{\alpha}_{o,l}|^2}. \quad (40)$$

Using (39) and (40), the root mean squared error (RMSE) is given by $\text{RMSE} = \sqrt{(\hat{O}_E - O_E)^2 + (\hat{O}_C - O_C)^2}$ where O_E and O_C are the true object extent and center-of-mass. The cumulative frequency of the RMSE for an SNR of $\frac{\|\mathbf{r} - \epsilon\|^2}{\|\epsilon\|^2} = -6$ dB is depicted in Figure 4a while the mean RMSE over SNR is depicted in Figure 4b. The proposed algorithm is able to outperform both SBL-based superresolution methods in terms of RMSE at all SNR levels, although the difference is more pronounced in low-SNR conditions of -3 dB and less. The reason for this becomes evident when investigating the histogram of the locations of detected components depicted in Figure 4c. While the mean number of components estimated in the object region is similar for the comparison methods, the proposed algorithms detects more components in the object region and is therefore able to estimate the parameters of the object more accurately. The increased number of estimated components is due to the lower threshold when adding new components within a group compared to adding new groups.

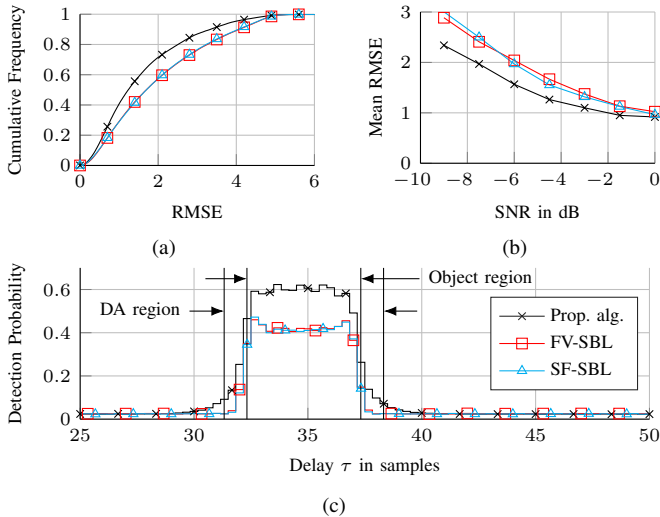


Fig. 4. Comparison of the proposed algorithm compared to the FV-SBL [38] and SF-SBL [36]. Cumulative frequency of the RMSE at an SNR of -6 dB (a), mean RMSE over SNR (b) and histogram of the delay of the detected components at an SNR of -6 dB (c).

Additional investigations not included in the paper revealed that the RMSE difference between the proposed algorithm and the comparison methods stems mainly from a more accurate estimation of the extent of the object while the estimation performance for the center-of-mass is similar for all three algorithms.

C. Variational Mode Decomposition

Another task which can be (approximately) solved by the proposed algorithm is VMD [8]. VMD decomposes a signal \mathbf{x} into several “intrinsic mode functions” \mathbf{x}_k

$$\mathbf{x} = \sum_{k=1}^K \mathbf{x}_k. \quad (41)$$

An “intrinsic mode function” $x_k(t) = A_k(t) \cos(\varphi_k(t))$ is defined in [8] as a sinusoidal function where the amplitude $A_k(t) \geq 0$ changes slowly over time t and the phase $\varphi_k(t)$ is a non-decreasing function with slowly time-varying instantaneous frequency $\frac{d\varphi_k(t)}{dt}$. Furthermore, we consider the discrete signal $\mathbf{x}_k = [x_k(-\frac{N}{2}T_s), x_k((-\frac{N}{2}+1)T_s), \dots, x_k((\frac{N}{2}-1)T_s)]^T$ sampled with regular intervals $f_s = \frac{1}{T_s}$. The model (41) is not an instance of (1). First, it considers real signals \mathbf{x} and \mathbf{x}_k instead of complex ones. However, This can be sidestepped by computing the discrete time analytical signal [47]. Secondly, (42) does not consider the signal to be embedded in additive noise. However, we find that modelling the noise is beneficial since noise is present in many practical applications anyway. Another difference between VMD and the algorithm developed here is, that VMD assumes the number of modes K is known a priori whereas the developed algorithm estimates K . Finally, it may not be immediately clear how to model each \mathbf{x}_k as a discrete sum of components. Since $x_k(t)$ is essentially an amplitude and phase modulated signal, almost all of the energy of the signal will be within a bandwidth which is much smaller than the sampling rate f_s . Therefore, each

$x_k(t)$ can be approximated by a signal with finite bandwidth which, by the sampling theorem, can be represented as a set of frequency samples (“tabs”) spaced with $\Delta f = \frac{f_s}{N}$. Thus, we approximate the discrete-time analytic signal of each mode as $\mathbf{x}_{a,k} \approx \sum_{l=-L_k}^{L_k} \alpha_{k,l} e^{j2\pi f_{k,l} t}$, where $f_{k,l} = \theta_k + l\Delta f$ and L_k relates to the bandwidth B_k of the k -th mode. The analytic signal \mathbf{x}_a is modeled as

$$\mathbf{x}_a \approx \sum_{k=1}^K \sum_{l=-L_k}^{L_k} \alpha_{k,l} e^{j2\pi f_{k,l} t} + \epsilon \quad (42)$$

which is an instance of (1). The original signals (or estimates thereof) can be obtained as the real part of the corresponding analytical signal. We used a larger search radius of $\mathcal{S}_{\text{search}} = \{\min(\hat{\mathcal{S}}_k) - 5, \min(\hat{\mathcal{S}}_k) - 4, \dots, \max(\hat{\mathcal{S}}_k) + 5\}$ due to the larger signal length and set $\chi_1 = 3$ dB as parameters for the proposed method. We set $\chi_2 = 10$ dB and $\chi_2 = 18$ dB for the 10 dB SNR and 30 dB SNR case, respectively, based on preliminary investigations.

To demonstrate the estimation accuracy of the underlying modes, we generate a signal of length $N = 1000$ samples consisting of two modes in AWGN according to (41). The amplitude and instantaneous frequency are defined at support points $t_m \in \{-\frac{N}{2}T_s, -\frac{N}{4}T_s, 0, \frac{N}{4}T_s, (\frac{N}{2}-1)T_s\}$ and linearly interpolated in between. The amplitude support points are defined as $A_{k,m} = A_{k,0}(1 + A_{\text{mod},k,m})$ where $A_{\text{mod},k,m} \sim \mathcal{U}(-A_{\text{mod},k}, A_{\text{mod},k})$ is a uniform random variable drawn independently for each mode k and support point m . Similarly, the instantaneous frequency at t_m is defined as $\frac{d\varphi_k(t)}{dt}|_{t=t_m} = 2\pi f_k(1 + f_{\text{mod},k,m})$ and linearly interpolated in between the points, where $f_{\text{mod},k,m} \sim \mathcal{U}(-f_{\text{mod},k}, f_{\text{mod},k})$ is again an i.i.d. uniform random variable. The phase $\varphi_k[n]$ is obtained by integrating the instantaneous frequency from $t = -\frac{N}{2}T_s$ to nT_s . We select the modulation parameters for the first mode to be $f_k = 0.1$, $f_{\text{mod},k} = 0.66$, $A_{k,0} = 1$ and $A_{\text{mod},k} = 0.25$ and for the second mode we select $f_k = 0.35$, $f_{\text{mod},k} = 0.03$, $A_{k,0} = 1$ and $A_{\text{mod},k} = 0.9$. Thus, the amplitude modulation is more pronounced in the second mode and the frequency modulation is more pronounced in the first mode. An example signal resulting from these settings is shown in Figure 5a.

We run a numerical simulation with $N_{\text{MC}} = 1000$ realizations of (41) with added real valued Gaussian noise ϵ of an SNR of $\frac{\|\mathbf{x}\|^2}{\|\epsilon\|^2} = 10$ dB representing a noisy signal and an SNR of 30 dB representing a (nearly) noiseless signal. We apply the proposed algorithm to the analytical signal and compare the estimation accuracy of the modes to the Matlab implementation (release R2022b) of the VMD algorithm. As performance metric we compared the estimation accuracy

$$\hat{e}_k = \min_l \frac{\|\mathbf{x}_k - \hat{\mathbf{x}}_l\|^2}{\|\mathbf{x}_k\|^2} \quad (43)$$

where \mathbf{x}_k are the true modes of the signal \mathbf{x} and $\hat{\mathbf{x}}_l$ are the estimated modes. Figures 5b and 5c depict the cumulative frequencies of the estimation error of both modes. The estimation performance of the proposed algorithm is better than the estimation performance of the VMD algorithm for both modes. However, it should be noted that the cumulative frequency of the estimation error “flattens out” at different values instead

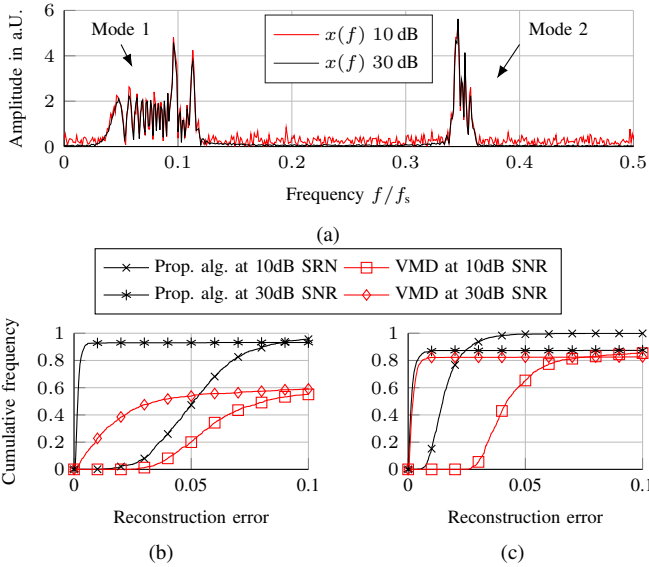


Fig. 5. Performance of the proposed algorithm for the task of VMD. (a) Example signal consisting of two modes, (b) cumulative frequency for the reconstruction error of mode 1 and (c) mode 2.

of converging towards 1, indicating some problem with the estimation process. Since the VMD algorithm was designed for narrowband modes, one reason for the poor estimation performance of the VMD algorithm on Mode 1 could be the large bandwidth of this mode. However, the proposed method was able to outperform the VMD algorithm even for the narrower second mode. The proposed algorithm overestimated the model order in 5% and 19% of the time for the 10 dB SNR case and 30 dB SNR case, respectively. In these cases, an additional mode appears, resulting in a significantly decreased estimation performance, which leads to the cumulative error frequency plateauing at a value < 1 .

Although we leave an extensive investigation of the performance of the proposed algorithm for VMD for future research, we chose to include these results to showcase how the algorithm can be applied to different problem settings.

VI. CONCLUSION

We derive an algorithm for the estimation of structured line spectra. Such structured line spectra can be found in many different fields, such as multi-pitch estimation, extended object detection using radar signals or VMD. Our algorithm is based on variational Bayesian inference and a Bernoulli-Gamma-Gaussian hierarchical prior model. In this model, the occurrence of groups is regularized by a Bernoulli prior while the occurrence of spectral lines is regularized by a Jeffrey's prior on the amplitude variances. Thus, a sparse estimate is obtained which automatically estimates the model order and the group structure in addition to the group parameters and component amplitudes. Due to the Bernoulli prior, the model is also more resilient to the insertion of additional artificial components compared to Gamma-Gaussian model used typically in SBL. The model can be straightforwardly adapted to a variety of inference problems based on the relation between the component frequencies $f_{k,l}$ and the group parameter θ_k .

We demonstrate the superior performance of our algorithm compared to state-of-the-art algorithms for multi-pitch estimation using numerical simulations and show that it is able to outperform state-of-the-art multi-pitch estimation algorithms when estimating the fundamental pitches in a major triad. Additionally, the developed algorithm is shown to outperform state-of-the-art model-based as well as pre-trained algorithms for multi-pitch estimation in accuracy, precision and recall when evaluated on the Bach-10 dataset. As a second example, we demonstrated how exploiting the structure of the underlying line spectra can be used to increase the estimation performance for the extent and center-of-mass of an extended object in low-SNR conditions compared to LSE algorithms for unstructured line spectra. As a third example, we detail how the proposed algorithm can be adapted to perform VMD and our algorithm is shown to outperform the Matlab implementation of the VMD algorithm in the presented example. However, a more extensive characterization of the performance of VMD should be performed by future research. These three examples demonstrate the versatility of the developed algorithm and show how integrating knowledge about the structural relations between spectral lines into the estimation procedure can lead to performance gains in the low SNR regime.

Promising directions for future research include the extension of the proposed algorithm to sequential processing based on belief propagation message passing [55], such as for radio-frequency simultaneous localization and mapping [56], [57], as well as using variational autoencoders [58] to learn arbitrary structured dictionaries.

APPENDIX

A. Derivation of the Variational Update Equations

For the derivation of q_α we insert (8) into (11). After taking the logarithm on both sides and ignoring all terms which do not depend on α , we get

$$\ln q_\alpha(\alpha; \hat{\theta}, \hat{z}) \stackrel{e}{\propto} \langle \ln p(x|\alpha, \theta = \hat{\theta}) + \ln p(\alpha|\gamma, z = \hat{z}) \rangle_{q_\lambda q_\gamma}. \quad (44)$$

Inserting (6) and (7) into (44) and ignoring all terms which do not depend on α , (44) can be rewritten as

$$\ln q_\alpha \stackrel{e}{\propto} \langle -\lambda(\mathbf{x} - \hat{\Psi}\alpha_\mathcal{S})^H(\mathbf{x} - \hat{\Psi}\alpha_\mathcal{S}) - \alpha_\mathcal{S}^H \mathbf{\Gamma} \alpha_\mathcal{S} + \sum_{\alpha_{k,l} \notin \alpha_\mathcal{S}} \ln \delta(\alpha_{k,l}) \rangle_{q_\lambda q_\gamma}. \quad (45)$$

Using the expectation of q_λ , i.e., $\hat{\lambda} = \langle \lambda \rangle_{q_\lambda}$ (see (17)) and the mean of $q_{\gamma,k,l}$, i.e., $\hat{\gamma}_{k,l} = \langle \gamma_{k,l} \rangle_{q_{\gamma,k,l}}$ (see (27)) and denoting the real operator as $\text{Re}\{\cdot\}$, (45) can be rewritten

$$\begin{aligned} \ln q_\alpha \stackrel{e}{\propto} & -(\alpha_\mathcal{S}^H (\hat{\lambda} \hat{\Psi}^H \hat{\Psi} + \hat{\mathbf{\Gamma}}) \alpha_\mathcal{S} - \text{Re}\{\alpha_\mathcal{S}^H 2\hat{\lambda} \hat{\Psi}^H \mathbf{x}\}) \\ & + \sum_{\alpha_{k,l} \notin \alpha_\mathcal{S}} \ln \delta(\alpha_{k,l}) \\ \stackrel{e}{\propto} & -(\alpha_\mathcal{S} - \hat{\alpha})^H \hat{\mathbf{C}}^{-1} (\alpha_\mathcal{S} - \hat{\alpha}) + \sum_{\alpha_{k,l} \notin \alpha_\mathcal{S}} \ln \delta(\alpha_{k,l}). \end{aligned} \quad (46)$$

After ‘‘completing the squares’’ using $\hat{\mathbf{C}} = (\hat{\lambda} \hat{\Psi}^H \hat{\Psi} + \hat{\mathbf{\Gamma}})^{-1}$ and $\hat{\alpha} = \hat{\lambda} \hat{\mathbf{C}} \hat{\Psi}^H \mathbf{x}$ we arrive at (12), (15) and (16) with q_α

being a complex Gaussian distribution of $\alpha_{\mathcal{S}}$ and $\alpha_{k,l} = 0$ for $\alpha_{k,l} \notin \alpha_{\mathcal{S}}$.

For the update of q_{λ} , we start again by inserting (8) into (11), applying the logarithm on both sides, and ignoring all terms which do not depend on λ , i.e.,

$$\ln q_{\lambda}(\lambda; \hat{\theta}, \hat{z}) \stackrel{e}{\propto} \langle \ln p(\mathbf{x}|\alpha, \theta = \hat{\theta}) + \ln p(\lambda) \rangle_{q_{\alpha} q_{\gamma}}. \quad (47)$$

Inserting the likelihood (7) and $p(\lambda) = \text{Ga}(\lambda|\rho, \mu)$ into (47), we get

$$\begin{aligned} \ln p_{\lambda} \stackrel{e}{\propto} & \langle \ln |\pi \lambda^{-1} \mathbf{I}| - \lambda(\mathbf{x} - \hat{\Psi} \alpha_{\mathcal{S}})^H (\mathbf{x} - \hat{\Psi} \alpha_{\mathcal{S}}) \\ & + (\rho - 1) \ln \lambda - \lambda \mu \rangle_{q_{\alpha} q_{\gamma}} \\ & \stackrel{e}{\propto} (N + \rho - 1) \ln \lambda - \lambda (\langle \|\mathbf{x} - \hat{\Psi} \alpha_{\mathcal{S}}\|^2 \rangle_{q_{\alpha}} + \mu). \end{aligned} \quad (48)$$

After solving the expectation of $\|\mathbf{x} - \hat{\Psi} \alpha_{\mathcal{S}}\|^2$ over q_{α} , we find that q_{λ} is again a Gamma distribution with shape $N + \rho$ and rate $\|\mathbf{x} - \hat{\Psi} \hat{\alpha}\|^2 + \text{tr}(\hat{\Psi} \hat{\mathbf{C}} \hat{\Psi}^H) + \mu$, as in (13) and (17).

For the derivation of $q_{\gamma,k,l}$ given that $\hat{z}_k = 1$, we again start with

$$\begin{aligned} \ln q_{\gamma,k,l}(\gamma_{k,l}; \hat{\theta}, \hat{z}) \stackrel{e}{\propto} & \langle \ln p(\alpha|\gamma, \mathbf{z} = \hat{z}) + \ln p(\gamma_{k,l}) \rangle_{q_{\bar{k}}} \\ & \stackrel{e}{\propto} \ln |\pi \Gamma^{-1}|^{-1} - \langle \alpha_{\mathcal{S}}^H \Gamma \alpha_{\mathcal{S}} \rangle_{q_{\bar{k}}} \\ & + (\eta - 1) \ln \gamma_{k,l} - \gamma_{k,l} \nu \end{aligned} \quad (49)$$

where $q_{\bar{k}}$ is the product of all the factors $q_k \in \mathcal{Q} \setminus \{q_{\gamma,k,l}\}$. Since $\Gamma = \text{diag}(\gamma_{\mathcal{S}})$, we can simplify $\ln |\pi \Gamma^{-1}|^{-1} = \ln \gamma_{k,l} + \text{const.}$ and $\alpha_{\mathcal{S}}^H \Gamma \alpha_{\mathcal{S}} = \gamma_{k,l} |\alpha_{k,l}|^2 + \text{const.}$ Thus, (49) can be rewritten as a Gamma PDF, i.e.,

$$\ln p_{\gamma,k,l} \stackrel{e}{\propto} \eta \ln \gamma_{k,l} - \gamma_{k,l} (|\hat{\alpha}_{k,l}|^2 + \hat{C}_{k,l} + \nu) \quad (50)$$

with shape $\eta + 1$ and rate $|\hat{\alpha}_{k,l}|^2 + \hat{C}_{k,l} + \nu$ as in (14) and (18). The derivation for $\hat{z}_k = 0$ is omitted because we consider it to be trivial.

B. Derivation of $\ln Z(\theta, z)$ and $\Delta_k(\theta_k)$

We start by showing that expression I in (20) is the logarithm of a complex Gaussian distribution for $\alpha_{\mathcal{S}}$ and $\alpha_{k,l} = 0$ for $\alpha_{k,l} \notin \alpha_{\mathcal{S}}$ plus an expressions which depends on θ and \mathbf{z} . Let $\Gamma_{\bar{\mathcal{S}}} = \text{diag}(\gamma_{\bar{\mathcal{S}}})$,

$$\begin{aligned} \text{I} &= \langle \ln p(\alpha, \theta, \gamma, \mathbf{z}, \lambda|\mathbf{x}) \rangle_{q_{\lambda} q_{\gamma}} \\ &\stackrel{e}{\propto} \langle -\lambda(\mathbf{x} - \Psi_{\bar{\mathcal{S}}} \alpha_{\mathcal{S}})^H (\mathbf{x} - \Psi_{\bar{\mathcal{S}}} \alpha_{\mathcal{S}}) + \ln |\pi \Gamma_{\bar{\mathcal{S}}}|^{-1} \\ &\quad - \alpha_{\mathcal{S}}^H \Gamma_{\bar{\mathcal{S}}} \alpha_{\mathcal{S}} + \ln p(\mathbf{z}) + \sum_{\alpha_{k,l} \notin \alpha_{\mathcal{S}}} \ln \delta(\alpha_{k,l}) \rangle_{q_{\lambda} q_{\gamma}}. \end{aligned} \quad (51)$$

After ‘‘completing the squares’’ and adding $\ln |\pi \mathbf{C}_{\bar{\mathcal{S}}}|^{-1} - \ln |\pi \mathbf{C}_{\mathcal{S}}|^{-1} = 0$ to complete the Gaussian distribution we find

$$\begin{aligned} \text{I} \stackrel{e}{\propto} & \ln |\pi \mathbf{C}_{\bar{\mathcal{S}}}|^{-1} - (\alpha_{\bar{\mathcal{S}}} - \hat{\alpha})^H \mathbf{C}_{\bar{\mathcal{S}}}^{-1} (\alpha_{\bar{\mathcal{S}}} - \hat{\alpha}) \\ & + \sum_{\alpha_{k,l} \notin \alpha_{\mathcal{S}}} \ln \delta(\alpha_{k,l}) + \hat{\lambda}^2 \mathbf{x}^H \Psi_{\bar{\mathcal{S}}} \mathbf{C}_{\bar{\mathcal{S}}} \Psi_{\bar{\mathcal{S}}}^H \mathbf{x} - \ln |\pi \mathbf{C}_{\bar{\mathcal{S}}}|^{-1} \\ & + \langle \ln |\pi \Gamma_{\bar{\mathcal{S}}}|^{-1} \rangle_{q_{\gamma}} + \ln p(\mathbf{z}) \\ & \stackrel{e}{\propto} \ln \mathcal{CN}(\alpha_{\bar{\mathcal{S}}}| \hat{\alpha}, \mathbf{C}_{\bar{\mathcal{S}}}) + \sum_{\alpha_{k,l} \notin \alpha_{\mathcal{S}}} \ln \delta(\alpha_{k,l}) + \ln p(\mathbf{z}) \\ & + \hat{\lambda}^2 \mathbf{x}^H \Psi_{\bar{\mathcal{S}}} \mathbf{C}_{\bar{\mathcal{S}}} \Psi_{\bar{\mathcal{S}}}^H \mathbf{x} - \ln |\mathbf{C}_{\bar{\mathcal{S}}}| + \sum_{\gamma_{k,l} \in \gamma_{\mathcal{S}}} \langle \ln \gamma_{k,l} \rangle_{q_{\gamma,k,l}}. \end{aligned} \quad (52)$$

Inserting (52) into (21), all terms which depend on α integrate to 1 since they form a valid distribution. Thus, after integrating out α and taking the logarithm we arrive at (25).

Let $\mathbf{C}_k = (\hat{\lambda} \Psi_k^H \Psi_k + \Gamma_k - \hat{\lambda}^2 \Psi_k \Psi_k^H \Psi_k \Psi_k^H \mathbf{C}_{\bar{k}} \Psi_k^H \Psi_k)^{-1}$, we express the covariance matrix $\mathbf{C}_{\bar{\mathcal{S}}}$ in $\ln Z([\hat{\theta}_{\bar{k}}, \theta_k], [\hat{z}_{\bar{k}}, 1])$ as a block matrix

$$\mathbf{C}_{\bar{\mathcal{S}}} = \begin{bmatrix} \mathbf{C}_{\bar{k}}^{-1} & \hat{\lambda} \Psi_{\bar{k}}^H \Psi_{\bar{k}} \\ \hat{\lambda} \Psi_{\bar{k}}^H \Psi_{\bar{k}} & (\hat{\lambda} \Psi_{\bar{k}}^H \Psi_{\bar{k}} + \Gamma_k) \end{bmatrix}^{-1} \quad (53)$$

and use the formula for block-matrix inversion to find $\ln |\mathbf{C}_{\bar{\mathcal{S}}}| = \ln |\mathbf{C}_{\bar{k}}| + \ln |\mathbf{C}_k|$ and

$$\begin{aligned} & \hat{\lambda}^2 \mathbf{x}^H \Psi_{\bar{\mathcal{S}}} \mathbf{C}_{\bar{\mathcal{S}}} \Psi_{\bar{\mathcal{S}}}^H \mathbf{x} \\ &= \hat{\lambda}^4 \mathbf{x}^H \Psi_{\bar{k}} \mathbf{C}_{\bar{k}} \Psi_{\bar{k}}^H \Psi_k \mathbf{C}_k \Psi_k^H \Psi_{\bar{k}} \mathbf{C}_{\bar{k}} \Psi_{\bar{k}}^H \mathbf{x} + \hat{\lambda}^2 \mathbf{x}^H \Psi_{\bar{k}} \mathbf{C}_{\bar{k}} \Psi_{\bar{k}}^H \mathbf{x} \\ & \quad + \hat{\lambda}^2 \mathbf{x}^H \Psi_k \mathbf{C}_k \Psi_k^H \mathbf{x} - \text{Re}\{2 \hat{\lambda}^3 \mathbf{x}^H \Psi_k \mathbf{C}_k \Psi_k^H \Psi_{\bar{k}} \mathbf{C}_{\bar{k}} \Psi_{\bar{k}}^H \mathbf{x}\} \end{aligned}$$

which simplifies to

$$\hat{\lambda}^2 \mathbf{x}^H \Psi_{\bar{\mathcal{S}}} \mathbf{C}_{\bar{\mathcal{S}}} \Psi_{\bar{\mathcal{S}}}^H \mathbf{x} = \hat{\lambda}^2 \mathbf{x}^H \Psi_{\bar{k}} \mathbf{C}_{\bar{k}} \Psi_{\bar{k}}^H \mathbf{x} + \mathbf{u}^H \mathbf{C}_k^{-1} \mathbf{u}. \quad (54)$$

Note, that $\mathbf{C}_{\bar{\mathcal{S}}}$ in the calculation of $\ln Z([\hat{\theta}_{\bar{k}}, \theta_k], [\hat{z}_{\bar{k}}, 0])$ equals $\mathbf{C}_{\bar{k}}$ in the calculation of $\ln Z([\theta_{\bar{k}}, \theta_k], [\hat{z}_{\bar{k}}, 1])$. The same holds for $\Psi_{\bar{\mathcal{S}}}$ and $\Psi_{\bar{k}}$, respectively. Thus, we insert (54) into (25) and arrive at (26) after a few algebraic manipulations.

REFERENCES

- [1] P. Stoica and R. Moses, *Spectral analysis of signals*. Upper Saddle River, NJ, USA: Pearson Prentice Hall, 2005.
- [2] E. Benetos, S. Dixon, Z. Duan, and S. Ewert, ‘‘Automatic music transcription: An overview,’’ *IEEE Signal Process. Mag.*, vol. 36, no. 1, pp. 20–30, Jan. 2019.
- [3] M. Müller, D. P. W. Ellis, A. Klapuri, and G. Richard, ‘‘Signal processing for music analysis,’’ *IEEE J. Sel. Topics Signal Process.*, vol. 5, no. 6, pp. 1088–1110, Feb. 2011.
- [4] M. G. Christensen and A. Jakobsson, *Multi-Pitch Estimation*, ser. Synthesis Lectures on Speech & Audio Processing, B. H. Juang, Ed. San Rafael, CA, USA: Morgan & Claypool, 2009.
- [5] M. G. Christensen, P. Stoica, A. Jakobsson, and S. Holdt Jensen, ‘‘Multi-pitch estimation,’’ *Signal Process.*, vol. 88, no. 4, pp. 972–983, Apr. 2008.
- [6] K. Granstrom, M. Baum, and S. Reuter, ‘‘Extended object tracking: Introduction, overview, and applications,’’ *J. Advances Inf. Fusion*, vol. 12, no. 2, pp. 139–174, Dec. 2017.
- [7] F. M. Schubert, M. L. Jakobsen, and B. H. Fleury, ‘‘Non-stationary propagation model for scattering volumes with an application to the rural LMS channel,’’ *IEEE Trans. Antennas Propag.*, vol. 61, no. 5, pp. 2817–2828, Jan. 2013.
- [8] K. Dragomiretskiy and D. Zosso, ‘‘Variational mode decomposition,’’ *IEEE Trans. Signal Process.*, vol. 62, no. 3, pp. 531–544, Feb. 2014.
- [9] R. Schmidt, ‘‘Multiple emitter location and signal parameter estimation,’’ *IEEE Trans. Antennas Propag.*, vol. 34, no. 3, pp. 276–280, Mar. 1986.
- [10] R. Roy and T. Kailath, ‘‘ESPRIT-estimation of signal parameters via rotational invariance techniques,’’ *IEEE Trans. Acoust., Speech, Signal Process.*, vol. 37, no. 7, pp. 984–995, Jul. 1989.
- [11] I. Ziskind and M. Wax, ‘‘Maximum likelihood localization of multiple sources by alternating projection,’’ *IEEE Trans. Acoust., Speech, Signal Process.*, vol. 36, no. 10, pp. 1553–1560, Oct. 1988.
- [12] M. Feder and E. Weinstein, ‘‘Parameter estimation of superimposed signals using the EM algorithm,’’ *IEEE Trans. Acoust., Speech, Signal Process.*, vol. 36, no. 4, pp. 477–489, Apr. 1988.
- [13] P. Stoica and Y. Selen, ‘‘Model-order selection: a review of information criterion rules,’’ *IEEE Signal Process. Mag.*, vol. 21, no. 4, pp. 36–47, Jul. 2004.
- [14] R. Tibshirani, ‘‘Regression shrinkage and selection via the LASSO,’’ *J. Roy. Statistical Soc.: Ser. B (Statistical Methodology)*, vol. 58, no. 1, pp. 267–288, 1996.
- [15] S. S. Chen, D. L. Donoho, and M. A. Saunders, ‘‘Atomic decomposition by basis pursuit,’’ *SIAM Rev.*, vol. 43, no. 1, pp. 129–159, Mar. 2001.

- [16] S. Mallat and Z. Zhang, "Matching pursuits with time-frequency dictionaries," *IEEE Trans. Signal Process.*, vol. 41, no. 12, pp. 3397–3415, 1993.
- [17] M. Tipping, "The relevance vector machine," in *Advances Neural Inf. Process. Syst.*, vol. 12. Denver, CO, USA: MIT Press, Nov. 29 – Dec. 4, 1999, pp. 652–658.
- [18] M. E. Tipping and A. C. Faul, "Fast marginal likelihood maximisation for sparse Bayesian models," in *Proc. 9th Int. Workshop Artif. Intell. and Statist.*, vol. R4, Key West, FL, USA, Jan. 03–06, 2003, pp. 276–283.
- [19] D. Shutin, T. Buchgraber, S. R. Kulkarni, and H. V. Poor, "Fast variational sparse Bayesian learning with automatic relevance determination for superimposed signals," *IEEE Trans. Signal Process.*, vol. 59, no. 12, pp. 6257–6261, Dec. 2011.
- [20] P. Stoica, P. Babu, and J. Li, "SPICE: A sparse covariance-based estimation method for array processing," *IEEE Trans. Signal Process.*, vol. 59, no. 2, pp. 629–638, Feb. 2011.
- [21] D. P. Wipf and B. D. Rao, "Sparse bayesian learning for basis selection," *IEEE Trans. Signal Process.*, vol. 52, no. 8, pp. 2153–2164, Aug. 2004.
- [22] D. P. Wipf, B. D. Rao, and S. Nagarajan, "Latent variable Bayesian models for promoting sparsity," *IEEE Trans. Image Process.*, vol. 57, no. 9, pp. 6236–6255, Sep. 2011.
- [23] M. Yuan and Y. Lin, "Model selection and estimation in regression with grouped variables," *J. Roy. Statistical Soc.: Ser. B (Statistical Methodology)*, vol. 68, no. 1, pp. 49–67, Feb. 2006.
- [24] M. Kyung, J. Gill, M. Ghosh, and G. Casella, "Penalized regression, standard errors, and Bayesian LASSOs," *Bayesian Anal.*, vol. 5, no. 2, pp. 369–411, Jun. 2010.
- [25] S. Raman, T. J. Fuchs, P. J. Wild, E. Dahl, and V. Roth, "The Bayesian group-LASSO for analyzing contingency tables," in *Proc. 26th Annu. Int. Conf. Mach. Learn.*, New York, NY, USA, Jun. 14–18, 2009, pp. 881–888.
- [26] X. Xu and M. Ghosh, "Bayesian variable selection and estimation for group LASSO," *Bayesian Anal.*, vol. 10, no. 4, pp. 909–936, Dec. 2015.
- [27] Y. Kim, J. Kim, and Y. Kim, "Blockwise sparse regression," *Statistica Sinica*, vol. 16, no. 2, pp. 375–390, Apr. 2006.
- [28] Y. C. Eldar, P. Kuppinger, and H. Bolcskei, "Block-sparse signals: Uncertainty relations and efficient recovery," *IEEE Trans. Signal Process.*, vol. 58, no. 6, pp. 3042–3054, Jun. 2010.
- [29] Z. Zhang and B. D. Rao, "Sparse signal recovery with temporally correlated source vectors using sparse bayesian learning," *IEEE J. Sel. Topics Signal Process.*, vol. 5, no. 5, pp. 912–926, 2011.
- [30] —, "Extension of SBL algorithms for the recovery of block sparse signals with intra-block correlation," *IEEE Trans. Signal Process.*, vol. 61, no. 8, pp. 2009–2015, Apr. 2013.
- [31] J. Fang, Y. Shen, H. Li, and P. Wang, "Pattern-coupled sparse bayesian learning for recovery of block-sparse signals," *IEEE Trans. Signal Process.*, vol. 63, no. 2, pp. 360–372, Jan. 2015.
- [32] T. Kronvall, S. I. Adalbjörnsson, S. Nadig, and A. Jakobsson, "Group-sparse regression using the covariance fitting criterion," *Signal Process.*, vol. 139, pp. 116–130, Oct. 2017.
- [33] Y. Chi, L. L. Scharf, A. Pezeshki, and A. R. Calderbank, "Sensitivity to basis mismatch in compressed sensing," *IEEE Trans. Signal Process.*, vol. 59, no. 5, pp. 2182–2195, May 2011.
- [34] M. F. Duarte and R. G. Baraniuk, "Spectral compressive sensing," *Appl. Comput. Harmon. Anal.*, vol. 35, no. 1, pp. 111–129, Jul. 2013.
- [35] Z. Yang and L. Xie, "On gridless sparse methods for line spectral estimation from complete and incomplete data," *IEEE Trans. Signal Process.*, vol. 63, no. 12, pp. 3139–3153, Jun. 2015.
- [36] T. L. Hansen, B. H. Fleury, and B. D. Rao, "Superfast line spectral estimation," *IEEE Trans. Signal Process.*, vol. 66, no. 10, pp. 2511–2526, Feb. 2018.
- [37] T. L. Hansen, M. A. Badiu, B. H. Fleury, and B. D. Rao, "A sparse Bayesian learning algorithm with dictionary parameter estimation," in *2014 IEEE 8th Sensor Array and Multichannel Signal Process. Workshop (SAM)*, A Coruna, Spain, Jun. 22–25, 2014, pp. 385–388.
- [38] D. Shutin, W. Wand, and T. Jost, "Incremental sparse Bayesian learning for parameter estimation of superimposed signals," in *10th Int. Conf. Sampling Theory and Appl.*, Bremen, Germany, Jul. 1–5, 2013, pp. 513–516.
- [39] M.-A. Badiu, T. L. Hansen, and B. H. Fleury, "Variational Bayesian inference of line spectra," *IEEE Trans. Signal Process.*, vol. 65, no. 9, pp. 2247–2261, May 2017.
- [40] N. L. Pedersen, C. Navarro Manchón, M.-A. Badiu, D. Shutin, and B. H. Fleury, "Sparse estimation using Bayesian hierarchical prior modeling for real and complex linear models," *Signal Process.*, vol. 115, pp. 94–109, Oct. 2015.
- [41] S. I. Adalbjörnsson, A. Jakobsson, and M. G. Christensen, "Multi-pitch estimation exploiting block sparsity," *Signal Process.*, vol. 109, pp. 236–247, Apr. 2015.
- [42] J. Sward, H. Li, and A. Jakobsson, "Off-grid fundamental frequency estimation," *IEEE/ACM Trans. Audio, Speech, Language Process.*, vol. 26, no. 2, pp. 296–303, Feb. 2018.
- [43] E. Vincent and M. D. Plumbley, "Efficient bayesian inference for harmonic models via adaptive posterior factorization," *Neurocomput.*, vol. 72, no. 1, pp. 79–87, Dec. 2008.
- [44] D. G. Tzikas, A. C. Likas, and N. P. Galatsanos, "The variational approximation for Bayesian inference," *IEEE Signal Process. Mag.*, vol. 25, no. 6, pp. 131–146, Nov. 2008.
- [45] C. M. Bishop, *Pattern Recognition and Machine Learning (Information Science and Statistics)*. Secaucus, NJ, USA: Springer-Verlag New York, Inc., 2006.
- [46] E. Leitinger, S. Grebien, B. Fleury, and K. Witrals, "Detection and estimation of a spectral line in MIMO systems," in *2020 54th Asilomar Conf. Signals, Syst. and Computers*, Pacific Grove, CA, USA, Nov. 01–04, 2020, pp. 1090–1095.
- [47] L. Marple, "Computing the discrete-time "analytic" signal via FFT," *IEEE Trans. Signal Process.*, vol. 47, no. 9, pp. 2600–2603, Sep. 1999.
- [48] D. Schuhmacher, B.-T. Vo, and B.-N. Vo, "A consistent metric for performance evaluation of multi-object filters," *IEEE Trans. Signal Process.*, vol. 56, no. 8, pp. 3447–3457, Aug. 2008.
- [49] Z. Duan, B. Pardo, and C. Zhang, "Multiple fundamental frequency estimation by modeling spectral peaks and non-peak regions," *IEEE/ACM Trans. Audio, Speech, Language Process.*, vol. 18, no. 8, pp. 2121–2133, Nov. 2010.
- [50] A. de Cheveigné and H. Kawahara, "YIN, a fundamental frequency estimator for speech and music," *J. Acoust. Soc. Amer.*, vol. 111, no. 4, pp. 1917–1930, Apr. 2002.
- [51] M. Bay, A. F. Ehmman, and J. S. Downie, "Evaluation of multiple-F0 estimation and tracking systems," in *Proc. 10th Int. Soc. Music Inf. Retrieval Conf.*, Kobe, Japan, Oct. 26 – 30, 2009, pp. 315–320.
- [52] F. Elvander, J. Sward, and A. Jakobsson, "Online estimation of multiple harmonic signals," *IEEE/ACM Trans. Audio, Speech, Language Process.*, vol. 25, no. 2, pp. 273–284, Feb. 2017.
- [53] E. Benetos and T. Weyde, "An efficient temporally-constrained probabilistic model for multiple-instrument music transcription," in *Proc. 16th Int. Soc. Music Inf. Retrieval Conf.*, Malaga, Spain, Oct. 26–30, 2015.
- [54] X. Li, Y. Yan, J. Soraghan, Z. Wang, and J. Ren, "A music cognition-guided framework for multi-pitch estimation," *Cogn. Comput.*, pp. 1–13, 2022.
- [55] X. Li, E. Leitinger, A. Venus, and F. Tufvesson, "Sequential detection and estimation of multipath channel parameters using belief propagation," *IEEE Trans. Wireless Commun.*, vol. 21, no. 10, pp. 8385–8402, Oct. 2022.
- [56] E. Leitinger, F. Meyer, F. Hlawatsch, K. Witrals, F. Tufvesson, and M. Z. Win, "A belief propagation algorithm for multipath-based SLAM," *IEEE Trans. Wireless Commun.*, vol. 18, no. 12, pp. 5613–5629, Dec. 2019.
- [57] E. Leitinger, A. Venus, B. Teague, and F. Meyer, "Data fusion for multipath-based SLAM: Combining information from multiple propagation paths," *ArXiv e-prints*, 2022. [Online]. Available: <https://arxiv.org/abs/2211.09241>
- [58] M. J. Johnson, D. K. Duvenaud, A. Wiltchko, R. P. Adams, and S. R. Datta, "Composing graphical models with neural networks for structured representations and fast inference," in *Advances Neural Inf. Process. Syst.*, vol. 29. Barcelona, Spain: Curran Associates, Inc., Dec. 5–10, 2016.